Non-Minimum-Phase Dynamics in the Electric Power Transmission Network: Identification, Analysis, and Preserving Model Reduction

Final Project Report

S-68G

Power Systems Engineering Research Center

Empowering Minds to Engineer
the Future Electric Energy System

Non-Minimum-Phase Dynamics in the Electric Power Transmission Network: Identification, Analysis, and Preserving Model Reduction (S-68G)

Final Project Report

Project Team

Sandip Roy, Project Leader
Vaithianathan (Mani) Venkatasubramanian
Kasra Koorehdavoudi, Graduate Student
Mohammadreza Hatami, Graduate Student
Washington State University

PSERC Publication #17-03

June 2017

For information about this project, contact

Sandip Roy
509-335-2448
sroy@eecs.wsu.edu

Power Systems Engineering Research Center

The Power Systems Engineering Research Center (PSERC) is a multi-university Center conducting research on challenges facing the electric power industry and educating the next generation of power engineers. More information about PSERC can be found at the Center's website: http://www.pserc.org.

For additional information, contact:

Power Systems Engineering Research Center
Arizona State University
527 Engineering Research Center
Tempe, Arizona 85287-5706
Phone: 480-965-1643
Fax: 480-727-2052

Notice Concerning Copyright Material

Acknowledgements

The investigators acknowledge the gracious support and collaboration of engineers at RTE-France (including Patrick Panciatici, Xavier Florent, and Florent Thibault), who not only sponsored the project research but also have been involved in every step of the project's technical development.

Executive Summary

Several factors including higher penetration of intermittent renewables, changing operational paradigms, and new technology deployment (e.g., power-electronic controls) are necessitating a fresh look at the fast dynamics of the bulk power transmission network, which extends beyond the traditional modal perspective. The purpose of this PSERC project, supported by RTE-France, was to initiate a study of the fast dynamics of the bulk power network from an input-output perspective. The focus was particularly on characterizing nonminimum-phase zeros, which essentially determine response properties and place fundamental limits on control. Several results were obtained, including: 1) topological conditions for the presence/absence of nonminimum-phase zeros; 2) understanding of the dependence of zeros on operating conditions; 3) demonstration that nonminimum-phase dynamics may be missed when standard model-reduction techniques are used; 4) characterization of the role of HVDC modulation on zeros; and 5) preliminary algorithm development for estimation of nonminimum-phase zeros from synhrophasor data. As a whole, the project research demonstrates that the presence of nonminimum-phase behaviors in the power grid's fast dynamics may be a real concern, depending on the structure and operating point of the grid.

Project Publications:

[1] Koorehdavoudi, Kasra, Mohammadreza Hatami, Sandip Roy, Vaithianathan Venkatasubramanian, Patrick Panciatici, Florent Xavier, and Jackeline Abad Torres. "Input-output characteristics of the power transmission network's swing dynamics." In Decision and Control (CDC), 2016 IEEE 55th Conference on, pp. 1846-1852., Las Vegas, Nevada, Dec. 2016.

[2] Koorehdavoudi, Kasra, Sandip Roy, Thibault Prevost, Florent Xavier, Patrick Panciatici, Vaithianathan Venkatasubramanian, ``Input-output properties of the swing dynamics for power transmission networks with HVDC modulation," to appear in the IFAC World Congress, Toulouse, France, June 2017.

[3] Mohammadreza Hatami, Vaithianathan Venkatasubramanian, Sandip Roy, Patrick Panciatici, Thibault Prevost, Florent Xavier, ``Study of nonminimum phase zeros in test power systems from wide-area control designs," to appear in the IREP 2017 Symposium, Espinho, Portugal, Aug.-Sep., 2017.

Student Theses: None completed (K. Koorehdavoudi and M. Hatami are pursuing research toward PhDs).

Table of Contents

Contents

List of Figures

List of Tables

1. Introduction

1.1 Background

New challenges are arising in understanding and controlling transients in the power transmission network [1]. First, a wide array of new devices and technologies are being deployed, which may subject the network to new types of disturbances while also modulating the network's dynamic responses. Second, increasing penetration of intermittent renewables is leading to increasing variability and uncertainty in the network's operating point and inertial characteristics, and hence also in its swing dynamics [2]. Specifically, generation units have increasingly diverse inertias, and the spatial pattern of inertia in the network is both changing from before and becoming more volatile depending on wind and solar conditions. In some cases, the incorporation of renewables is also further stressing the network since these generators are located far from load centers, and myriad other stressors are complicating power-grid operations. The increased stress may lead to more extensive swings [3].

At the same time, new sensors, power-electronics-based actuators, and communication capabilities are being integrated into the electric power grid. In consequence, control of transients in the power transmission network is evolving from a local and specialized paradigm, toward one where many generic sensors and actuators across a wide area are being used in tandem [1,4]. While this changing paradigm may bring forth many benefits (e.g. in damping oscillations and other transients, addressing fault scenarios, increasing flexibility, etc.), it also necessitates new simulations, formal analyses, and control design techniques.

Designing wide-area controls and evaluating propagative transients in the bulk power transmission network requires understanding input-output properties of the network's swing dynamics [5], as a foundational step. That is, it is necessary to understand the relationship between a putative input at one location in the network (whether an actuation signal or an unknown disturbance) and the swing-dynamics response at another network location (whether a measurement signal used in feedback or a response variable of interest). These behaviors are essentially codified in the *zeros* or *zero dynamics* of the transfer models describing the input-output relationships.

There is a very wide literature in the controls community on zeros and their implications on system dynamics and control [6]. A main outcome of this research is the realization that the locations of zeros, and particularly the absence or presence of nonminimum-phase zeros, play a crucial role in disturbance responses and controls. While electric power system transients are typically not analyzed from an input-output perspective, Martins and his co-workers have voiced the importance of input-output analyses, and pursued the numerical computation of zeros in a sequence of studies (e.g., [7]). These efforts focus particularly on the computation of zeros for differential-algebraic-equation (singular system) models for the swing dynamics, and follow on analyses of zeros for singular systems in the control community [8,9]. While these various studies provide a starting point for analyzing the zeros of swing-dynamics models, they do not provide a comprehensive structural understanding of zeros in analogy with the modal analysis of the swing dynamics. Such a structural understanding is necessary for addressing the emerging challenges in evaluating/managing transients, and leveraging new technologies for wide-area control.

The research pursued in this project is particularly aligned to a recent literature on the input-output dynamics of dynamical networks. These efforts have been concentrated on tying the zero locations of canonical linear network models (e.g., models for consensus, disease spread, etc.) to the network's topology [10-14]. Our research also builds on a wide and growing literature that approaches power-system transients analysis from a graph-theory perspective (e.g. [15-17]).

1.2 Overview of the Problem

As motivated in the background section above, changes in grid operations including new power electronic controls and growing renewables penetration are necessitating new understandings of the fast dynamics of the power grid, from an input-output perspective. The impacts of changing operations on the fast dynamics are manifesting in diverse locations – for instance, in the 2012 blackout in the Indian power grid, the cyber-attack impacts in Ukraine, oscillations noted by the New-England Independent System Operator (NEISO), and wide-area swings observed in the continental European grid, among many other instances. Particularly relevant to this project, several concerns about oscillations and transients are of interest to the project sponsors, RTE-France. These include: issues related to HVDC modulation on the France-Spain interchange, and concerns arising from integration of intermittent renewables (e.g., planned offshore wind farms) and the attendant variability in network operating points.

Based on these motivations, the main problem addressed in this project was to characterize the input-output properties of the power-system's swing dynamics, so as to support analysis/control of oscillations and transients. This broad problem involved solving four more specific problems. First, we sought to characterize input-output properties of the linearized swing dynamics – specifically, the locations of zeros (including the presence/absence of nonminimum-phase zeros) – in terms of the structure of the model. That is, we aimed to determine what features in the topology and physics of the power grid, and what placement of sensors and actuators, yielded minimum-phase or nonminimum-phase dynamics. Second, we studied what role HVDC modulation would have on input-output channels in the grid. Based on these characterizations, we then pursued two exploratory studies, which inform operational understanding and management of the swing dynamics, these exploratory studies were focused on: learning input-output properties from synchrophasor data; and determining whether or not model reduction techniques maintained input-output characteristics.

Main Issues

The project research was structured to answer several key questions about the fast dynamics of the electric power grid:

1) Is the presence of nonminimum-phase dynamics on control/disturbance channels indeed a practical and significant concern in operating the grid?

2) How do zero locations, and particularly the presence/absence of nonminimum zeros, depend on the parameters of the grid (including the topology, inertia and damping levels, the location of

the channel of interest relative to the topology, and the loading)? Can operational variability cause the network to switch from nonminimum phase to minimum phase?

3) How do HVDC line controls modify input-output properties of the swing dynamics? Specifically, can HVDC modulation cause the concurrent channel, or other channels of interest, to become nonminimum-phase, such that additional control may induce oscillatory or unstable dynamics?

4) Do standard model reduction techniques adequately maintain input-output properties? In particular, can model reduction techniques introduce or remove nonminimum phase zeros?

5) Good methods have been developed for the estimation of modes from synchrophasor data. Are there parallel approaches for identifying zeros from synchrophasor data?

Secondary Issues

Beyond the main questions related to transients and oscillations studied in the project (as discussed in Section 1.2.1), several secondary issues were also considered. These secondary issues were either methodological in nature, or more advanced issues related to power system dynamics that were only addressed in a preliminary way in the project. Secondary issues included:

1) Understanding how graph-theory ideas can be brought to bear to gain insight into the input-output dynamics, in parallel with the graph-theoretic methods developed for emergence in networks,

2) Comparing approaches for computing zeros, e.g. Laplace domain approaches, generalized eigenvalue-based approaches, and true eigenvalue-problem reformulations.

3) Developing bounds on model parameters that yield nonminimum-phase dynamics or guarantee minimum-phase dynamics.

4) Understanding dependences of zeros on parameters of interest from a root-locus viewpoint.

1.3 Report Organization

Section 2 of the report summarizes and illustrates the main project outcomes, so as to give the reader a quick overview of the scope and significance of the project, and pointers to more detailed results. Section 3 presents a self-contained treatment of the analytical results on zeros obtained for the classical model, and the extended results that address HVDC modulation. Section 4 complements the analytical treatment with a numerical study of zeros, for a more detailed model of a test system. Next, Section 5 presents results related to estimation of zeros from synchrophasor data. Finally, a brief conclusion is given in Section 6.

2. Summary of Project Outcomes

During 2016, the project investigators at Washington State University, in collaboration with RTE-France, studied the input-output properties of the power system's swing dynamics from a structural perspective. These structural analyses were also used to gain some preliminary insight into control analysis and design of the bulk power grid. These outcomes were reported in detail in three publications, which are attached as an appendix to this report. In this section, the main outcomes and methods are briefly summarized, so as to give the reader an overall perspective on the project scope.

The following main outcomes were achieved:

1) The classical linearized differential-algebraic equation (DAE) model for the swing dynamics was enhanced to represent input-output channels, as a starting point for the analysis of input-output properties. Specifically, the classical model was enhanced to represent an electrical power input at a single bus (as an abstraction of e.g. a governor control, a mechanical or electrical disturbance, or other control input). Also, the model was enhanced to explicitly represent a measurement of the (relative) angle or frequency at a single bus (as may be obtained via a synchrophasor or a traditional sensor), which may in general be remote from the input location. Motivated by the recognition that HVDC modulation can significantly alter fast dynamics across a wide area, the classical model was also extended to represent HVDC modulation.

2) The invariant zeros of the input-output dynamics were characterized in terms of the power network's topology, for the developed input-output model. Specifically, we studied how the presence/absence of nonminimum-phase zeros depend on parameters of the power network, including generator dampings and inertias, and the network's topology (line susceptances). The influence of changing operating points on the zeros was also examined. This structural analysis of the invariant zeros was undertaken using a transformation of linear systems known as the *special coordinate basis*. Importantly to the study here, the special coordinate basis allows the analysis of zeros to be phrased as an eigenvalue problem for a *zeros-state matrix*, which can be computed as a structured perturbation of a submatrix of the system's state matrix. This special eigenvalue perspective on the zeros readily allows characterization in terms of the topology and other structural parameters of the swing-dynamics model. A comprehensive development of such structural results, and an explanation of the special-coordinate-basis methodology, is contained in the attached publications. A main finding of these studies is that the nonminimum-phase zeros result when short weak (low-susceptance) paths and long strong (high-susceptance) paths connect the input and output. The analyses of parametric dependences also verify that realistic changes in network parameters (e.g., inertias) can cause control channels of interest to shift from minimum phase to nonminimum phase: particularly, nonminimum-phase behaviors become pronounced in networks with low damping, high congestion, and certain inertial structures, hence changes in power-system operations toward intermittent-renewables-rich configurations can indeed cause nonminimum-phase behaviors. Sample results are shown in Figure 1.

3) The impact of HVDC modulation on collocated input-output dynamics was determined. This analysis was also based on the special coordinate basis transformation, but required further effort to understand how the parameters of the in-built HVDC controller modified the zeros of the channel of interest. In particular, it was found that proportional and proportional-derivative controls can be systematically designed to achieve minimum-phase dynamics, with high-gain designs achieving minimum-phase behaviors. However, these high-gain designs are especially sensitive to delays in measurements used for HVDC modulation. Thus, if measurement delays are present, appropriate filtering is needed. Sample results are shown in Figure 2.

4) An example was developed which shows that input-output properties of the swing dynamics may not be preserved when standard model reduction techniques are used, see Figure 3. In particular, the example shows that the standard slow-coherency-based model reduction may eliminate a non-minimum-phase zero in a control channel of interest, such that a nonminimum-phase dynamics appears minimum phase. Likewise, balanced-truncation-based model reduction techniques are not guaranteed to maintain input-output characteristics. Beyond developing the example, a literature survey was conducted on methods for input-output-dynamics preserving model reduction. While some preliminary work has been done in these directions, developing systematic model reduction techniques that maintains zeros as well as topological properties is a main direction of outstanding work.

5) An initial exploration of estimation of zeros from synchrophasor data was conducted. Specifically, estimation of input-output transfer functions from impulse-response data, as obtained from Chief Jo generator brake tests and Pacific DC Inter-tie (PDCI) noise probing tests, was undertaken. This initial exploration demonstrated that estimation of transfer function zeros from impulse-response data is more difficult in comparison to estimation of modes (i.e., transfer-function poles). Following on this initial study, we have begun a systematic study of zeros estimation of linear systems from ambient data: initial results confirm that the estimation of zeros is hard compared to the estimation of poles, however multi-channel data can surprisingly improve zero estimation for a particular channel.

6) Input-output properties were evaluated for a small model of part of the French power network. In particular, a 64-bus planning model for Northwest France was considered, which incorporates envisioned off-shore wind generation. These simulations show the strong dependence of input-output properties on the network loading, and also on the locations of the inputs and outputs relative to the network topology. In particular, it was found that transfer functions across long offshore-onshore lines were nonminimum-phase under heavy loading conditions. Sample results are shown in Figure 4.

These outcomes of the project have been described in detail in three publications, which are attached as an appendix to this work.

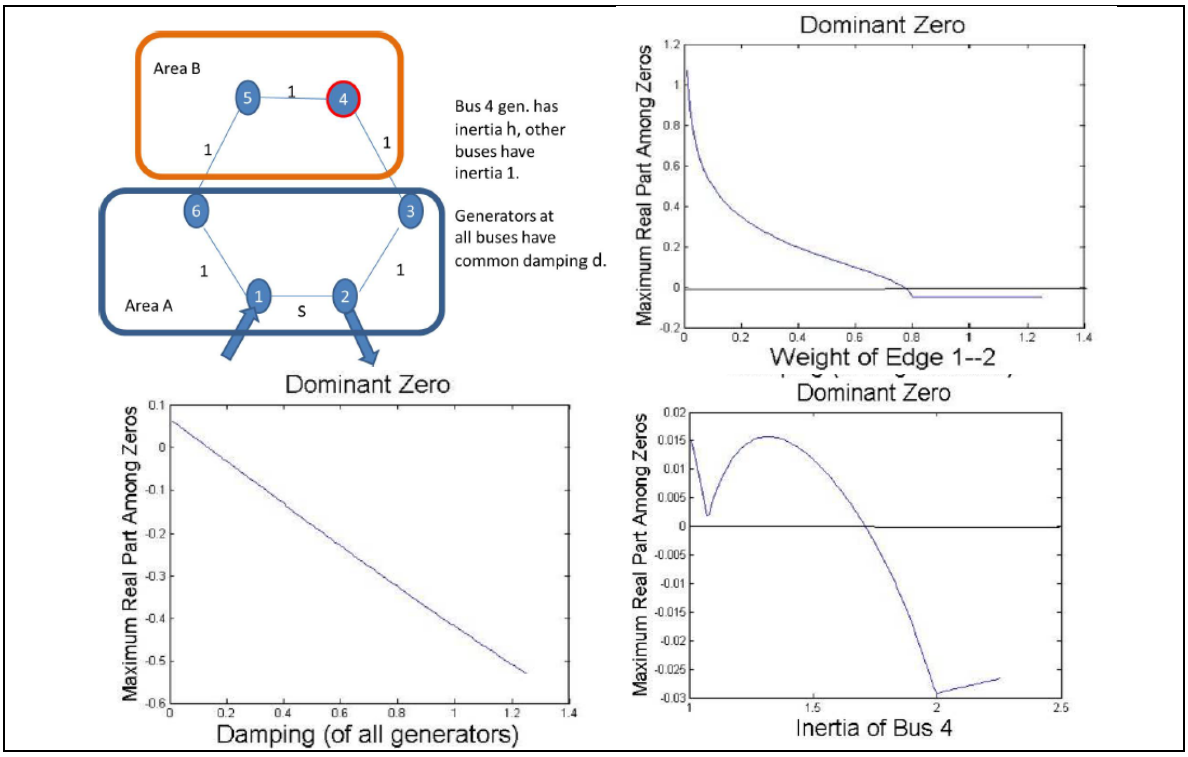

Figure 1: The dependences of swing-dynamics zeros on network model parameters, including topological parameters, and generator damping and inertia, were evaluated.

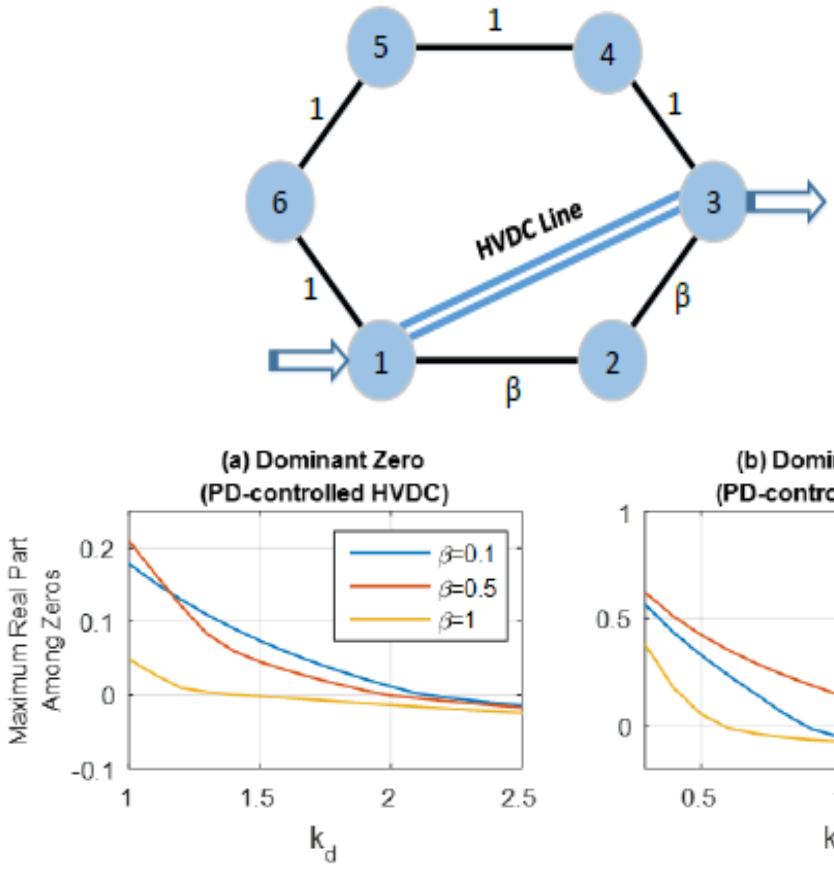

Figure 2: The analysis of input-output properties (specifically, invariant zeros) was extended to encompass power networks with HVDC modulation.

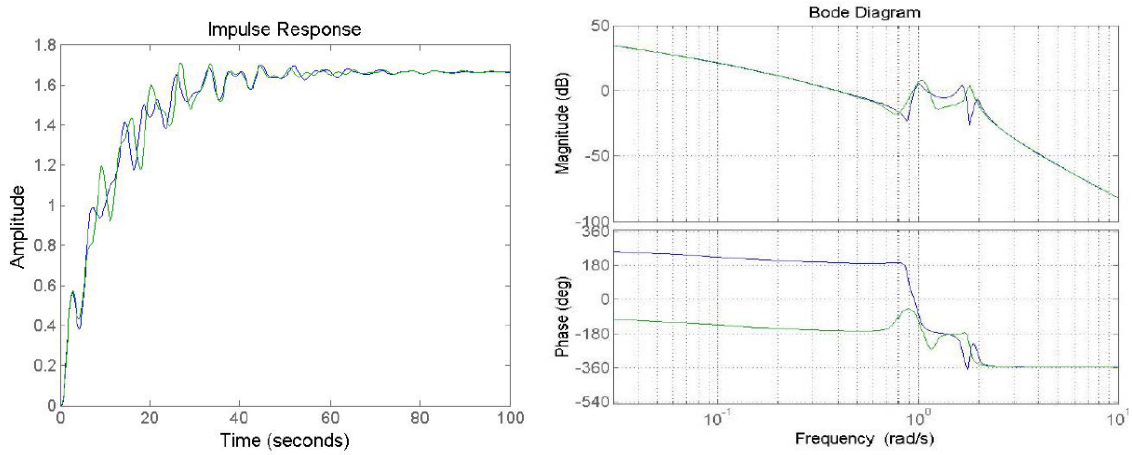

Figure 3: An exploratory example was pursued during the first project year, which demonstrates that standard model-reduction techniques for the swing dynamics may not preserve nonminimum-phase input-output dynamics.

Load	0	Low	medium	high	very high
	in-out	in-out	in-out	in-out	in-out
pair of non-minimum phase nodes	1 7	1 2	1 2	1 2	1 2
	7 1	1 8	2 1	1 7	1 7
		2 1	2 4	2 1	2 1
		2 4	2 6	2 4	2 4
		2 6	3 4	2 6	2 6
		3 4	4 2	3 4	4 2
		4 2	4 7	4 2	4 3
		4 8	6 2	4 5	4 5
		6 2	7 1	4 7	4 7
		6 8	7 4	6 2	4 8
		7 1		7 1	5 1
		7 4		7 4	5 4
					6 2
					7 1
					7 4
					8 4

Figure 4: The zeros analysis has been applied to a model of part of the French transmission network. Here, the nonminimum-phase pairs are shown for different loading levels. Transfer functions between offshore wind generator buses and nuclear generator buses are often nonminimum phase.

3. Analysis of Zeros for the Classical Model without and with HVDC Modulation

3.1. Overview of the work done

The bulk power transmission network is being subject to increasing stress and uncertainty due to renewables integration, changing regulatory paradigms, and use of new devices and technologies (e.g., power electronics, new protection devices, complex distribution technologies, syncrophasors), among other reasons (see [1-4]). This increased stress and variability is complicating the analysis and control of transients/oscillations in the grid, and necessitating network-theoretic analysis of disruptions as well as wide-area control strategies. Analyzing disruptions and designing wide-area controls, at its essence, requires understanding input-output properties of the power network's swing dynamics. A natural first step is to study the classical swing-dynamics model [5], which uses two state variables for each intertial generator, from an input-output perspective. There is a particular interest in developing structural or graph-theoretic insights into the input-output dynamics, and specifically the invariant zeros of this dynamics, as a means to understand how network parameters impact input-output properties, and obtain simple rubrics for analysis and control design. The main purpose of this work is to: 1) explore the input-output properties of the swing dynamics from an algebraic standpoint; 2) develop structural and graph-theoretic results into the zeros of the input-output swing dynamics model (focusing particularly on conditions for minimum-phase dynamics); and 3) and expand this analysis framework to encompass networks with controlled high-voltage direct-current (HVDC) lines.

The analysis of input-output dynamics developed here informs, particularly, the deployment and design of controllers for HVDC lines. While the bulk power transmission network primarily uses alternating current (AC), HVDC lines are appealing for transmission of large amounts of power over long distances, as well as for other applications including long-distance underwater transmission and asynchronous linking of two AC systems, because they can alleviate congestion and alter operating points significantly, HVDC lines can have large impact on the stability and transient characteristics of power networks. Also, the integration of solid-state power electronics and synchrophasors is enabling sophisticated fast control of HVDC lines (known in the literature as HVDC *modulation*). However, experience shows that HVDC modulation needs to be undertaken with care, since these controls can introduce oscillations or leave the network susceptible to disruptions (see [18,19]). The analysis of control channels pursued here directly informs the design and analysis of controllers for HVDC lines.

In this study, we concentrate on single-input single-output (SISO) channels in linearized models of the power-system swing dynamics, but approach the analysis in a way that generalizes to more complex input-output structures. First, we focus on developing the algebraic machinery that enables structural and graph-theoretic characterization of the zeros. Second, the algebraic machinery is used to develop several basic graph-theoretic conditions for minimum-phase input-output dynamics. As primary results of this part, it is shown that the dynamics are minimum-phase if: 1) the input and output are collocated, 2) there is a single path between the input and output in the network graph, 3) the shortest input-output path is sufficiently strong compared to alternative paths, or 4) the generators have high damping. Third, we pursue the input-output analysis when controlled HVDC lines are present. As primary results of this part, it is shown that the dynamics

are minimum-phase if the HVDC line between input and output nodes has proportional or derivative controller with high gain. On the other hand, it is shown that proportional and lag compensation schemes with sufficient gain yield nonminimum-phase transfer functions, if measurement delays are present.

The research described here contributes to a recent research thrust in the controls community, on characterizing the zeros of canonical linear network models (e.g., models for disease spread, consensus, etc) from a graph-theory perspective (see [10-14]). The initial studies in this direction were focused on models with scalar subsystem dynamics, and were subsequently extended to include models with homogeneous vector subsystems. Compared to these previous efforts, this study focuses on a heterogeneous dynamical-network model, and develops structural results that are specially related to power-system analysis. The work presented here also gives insight into the impact of control schemes in a network (specifically, HVDC controls) on input-output channel characteristics. Our research also builds on a wide literature which approach power-system small-signal and transient analysis from a graph-theory perspective (e.g. see [15,17])

The rest of the article is organized as follows. In Section 3.2, the input-output swing-dynamics model is reviewed, and also enhanced to represent controlled HVDC lines. In Section 3.3, the input-output properties of the swing dynamics is analyzed from an algebraic standpoint (Section 3.3.1), several structural and graph-theoretic results on the zeros of the nominal swing-dynamics model are given (Section 3.3.2), and then the dependence of input-output characteristics on HVDC controls is examined (Section 3.3.3). Several examples are presented to illustrate the results, and give an indication of parameter thresholds that distinguish minimum-phase and non-minimum-phase behaviors (Section 4). *Due to space constraints and the tutorial focus of this report, proofs of all the theorems are excluded, see [20,21]).*

3.2. Modeling

Input-output properties of the classical linearized swing dynamics model for the power transmission network are considered. The classical linearized swing dynamics model uses two state variables (the electrical angle and frequency relative to a reference) at the buses with inertial generators. A single input-output channel is imposed on the model, where the input is abstractly modeled as a power injection/extraction at a single bus, and the output is a frequency or angle measurement at a single (possibly different) bus. Formally, the following model is considered:

$$\begin{bmatrix}\dot{\delta}\\ \dot{\omega}\end{bmatrix} = \begin{bmatrix}0 & I\\ -H^{-1}L(\Gamma) & -H^{-1}D\end{bmatrix}\begin{bmatrix}\delta\\ \omega\end{bmatrix} + \begin{bmatrix}0\\ \mathbf{e}_i\end{bmatrix}u \qquad (1)$$

$$y = \begin{bmatrix}0 & \mathbf{e}_j^T\end{bmatrix}\begin{bmatrix}\delta\\ \omega\end{bmatrix}$$

where

$$\delta(t) = \begin{bmatrix}\delta_1 & \cdots & \delta_n\end{bmatrix}^T,$$

represents the differential electrical angles at the *n* buses at time *t* (relative to a nominal trajectory),

$$\omega(t) = \begin{bmatrix} \omega_1 & \cdots & \omega_n \end{bmatrix}^T$$

represents the differential electrical frequencies at the buses, the notation $\mathbf{e}_q$ represents a 0-1 indicator vector with qth entry equal to 1, the scalar input $u(t)$ is a power-injection signal at bus i, and the scalar output $y(t)$ is the frequency at bus j.

The model is defined by the following parameters: the positive diagonal matrix H represents the inertias of the generators at the buses, the positive diagonal matrix D captures the dampings of the generators, and the matrix $L(\Gamma)$ is a symmetric positive-definite or positive semi-definite matrix that entirely specifies the interactions among the buses. Importantly, the zero pattern and nonzero entries in the matrix $L(\Gamma)$ are commensurate with the topology of the power transmission network (equivalently, electrical connectivity among the buses), as specified by the graph Γ. Specifically, Γ is defined to be an undirected weighted graph whose vertices represent the buses. The edge weights are the susceptances of the lines connecting the buses, provided that the linearization is around a unloaded operating condition; when the linearization is around a non-zero operating point, the edge weights are instead the susceptances scaled by the cosine of the nominal electrical-angle difference between the vertices ([5]); these “effective susceptances" capture the changed stiffnesses in the swing dynamics. Each off-diagonal entry of the matrix $L(\Gamma)$ equals the negative of the edge weight between the corresponding vertices if there is an edge, and equals zero otherwise. The diagonal entries of $L(\Gamma)$ are positive, and at least as large as the absolute sum of the off-diagonal entries on the corresponding row or column. We assume throughout the section that Γ is connected.

For convenience, we use the notation A for the state matrix of the system, i.e.,

$$A = \begin{bmatrix} 0 & I \\ -H^{-1}L(\Gamma) & -H^{-1}D \end{bmatrix}.$$

We also find it convenient to define the state vector of the swing-dynamics model as

$$\mathbf{x} = \begin{bmatrix} \delta \\ \omega \end{bmatrix}.$$

It can easily be checked that the matrix A is stable, in these sense that all eigenvalues are in the closed left half plane with no defective eigenvalues on the $j\omega$-axis. In fact, it can be checked that all eigenvalues of A are in the open-left half plane (OLHP), except that there is one eigenvalue at the origin in the special case that $L(\Gamma)$ is a true Laplacian matrix (all row sums are zero). The graph Γ is referred to as the **network graph**. Also, the nodes in the network where the input is applied and the output is measured (i and j, respectively) are referred to as the input and output nodes, and the corresponding vertices in the graph are referred to the the input and output vertices. The simplified model for the swing dynamics considered here is widely used in the power-engineering community ([5]), and constitutes a linearization of nonlinear Kuramoto oscillator-type model for the swing dynamics ([22]).The formulation assumes that all buses have inertial generation associated with them, or in other words that the loads-only buses have been reduced via solution of the algebraic equations in the swing dynamics (which requires a Kron reduction). The graph Γ represents the interconnectivity of this reduced model, not the original topology including the load buses. We focus on this case with the aim of understanding input-output dynamics among the major swinging components of the wide-area network. Developing analyses of zeros in terms of the original rather than reduced network model is left to future work. Here, the classical swing-

dynamics model is extended to capture the fast dynamics of high-voltage direct-current (HVDC) lines in the network. The effects of HVDC line controllers on small-signal behaviors are more intricate, and require modifying the classical swing-dynamics modeling framework. Since controllers across HVDC lines have been shown to influence small-signal properties, a major focus of this work will be to model and evaluate possible HVDC line controllers. Broadly, the fast controlled HVDC line included network is different from classical swing-dynamics model by having 1) new state and/or 2) new dependencies between states (new nonzero entries in the state matrix). Small signal models for fast controlled HVDC have been described in ([18,19]). Here, four control schemes of increasing sophistication are modeled. We focus particularly on the case that the transfer function between the two ends of the HVDC line is of interest, i.e. the HVDC line is integrated between the input and output. This case is of particular interest because it shows whether or not inclusion of a HVDC line can improve small-signal characteristics across a channel of interest (typically one that is highly congested), and allow analysis of disruptions associated with the HVDC line. Here are the models:

1) A HVDC line with fixed power (no feedback regulation of power) does not alter the small-signal model, beyond changing graph edge weights (stiffnesses) due to the altered power flow.

2) A HVDC line may use a proportional controller, for which the power input is regulated using a proportional (P) feedback control of the electrical phase angle difference across the DC line ($P_{in}=k(\delta_j-\delta_i)$, where P_{in} is the differential power injection to bus i and extraction from bus j). An HVDC line with proportional control can be captured in the swing-dynamics model by including additional non-zero entries in L matrix, identically to a newly added AC line. Precisely, when a proportional-controlled HVDC line with gain k is included between buses i and j, the nominal linear swing dynamic models is modified by adding k to $L_{i,i}$ and $L_{j,j}$ and adding $-k$ to $L_{i,j}$ and $L_{j,i}$. In this case, the linearized model of the HVDC line is identical to that of an AC line. Using the notation L_{DC} for the modification of the L matrix, the swing-dynamics model becomes:

$$\begin{bmatrix}\dot{\delta}\\ \dot{\omega}\end{bmatrix} = \begin{bmatrix}0 & I\\ -H^{-1}L_{DC}(\Gamma) & -H^{-1}D\end{bmatrix}\begin{bmatrix}\delta\\ \omega\end{bmatrix} + \begin{bmatrix}0\\ \mathbf{e}_i\end{bmatrix} u \text{ and } y = \begin{bmatrix}0 & \mathbf{e}_j^T\end{bmatrix}\begin{bmatrix}\delta\\ \omega\end{bmatrix}.$$

3) A proportional-derivative controller may be used for HVDC modulation. In this case, the power input is regulated using a proportional-derivative (PD) feedback of the electrical phase angle difference across the DC line (in Laplace domain, $P_{in}(s)=(k_p+k_ds)(\delta_j(s)-\delta_i(s))$, where P_{in} is the differential power injection to bus i and extraction from bus j). A HVDC line with PD controller can be captured in the swing-dynamics model, by introducing new non-zero entries in the L matrix, and changing the D matrix. Specifically, if a PD-controlled HVDC line is included between buses i and j, the linear swing dynamic model is modified by: 1) adding k_p to the entries $L_{i,i}$ and $L_{j,j}$ of L; 2) adding $-k_p$ to the entries $L_{i,j}$ and $L_{j,i}$ of L; 3) adding k_d to the entries $D_{i,i}$ and $D_{j,j}$ of D; 4) adding $-k_d$ to entries $D_{i,j}$ and $D_{j,i}$ of D. We call the updated L and D matrices as L_{DC} and D_{DC}, respectively. Hence, the linear model for this system is:

$$\begin{bmatrix}\dot{\delta}\\ \dot{\omega}\end{bmatrix} = \begin{bmatrix}0 & I\\ -H^{-1}L_{DC}(\Gamma) & -H^{-1}D_{DC}\end{bmatrix}\begin{bmatrix}\delta\\ \omega\end{bmatrix} + \begin{bmatrix}0\\ \mathbf{e}_i\end{bmatrix} u \text{ and } y = \begin{bmatrix}0 & \mathbf{e}_j^T\end{bmatrix}\begin{bmatrix}\delta\\ \omega\end{bmatrix}$$

4) Finally, a HVDC line with a lead-lag compensator is considered. In this case, the power input is regulated using a lead-lag compensated feedback of the electrical phase angle difference across the DC line (in Laplace form $P_{in}(s)=k\frac{1+T_1 s}{1+T_2 s}(\delta_j(s)-\delta_i(s))$, where P_{in} is the differential power injection to bus i and extraction from bus j). Representing lead-lag controllers in the swing-dynamics state-space model requires a new state variable, and new connections among state variables. The following is the linear swing-dynamics model with lead compensator included. The full swing model can be expressed by enhancing the original model to include an additional dynamic feedback:

$$\begin{bmatrix}\dot{\delta}\\ \dot{\omega}\end{bmatrix}=\begin{bmatrix}0 & I\\ -H^{-1}L(\Gamma) & -H^{-1}D\end{bmatrix}\begin{bmatrix}\delta\\ \omega\end{bmatrix}+\begin{bmatrix}0\\ -H^{-1}\mathbf{e}_{j,i}\end{bmatrix}P+\begin{bmatrix}0\\ \mathbf{e}_i\end{bmatrix}u \qquad (2)$$

$$T_2\dot{P}=-P+k\begin{bmatrix}\mathbf{e}_{j,i}^T & T_1\mathbf{e}_{j,i}^T\end{bmatrix}\begin{bmatrix}\delta\\ \omega\end{bmatrix}\quad,\quad y=\begin{bmatrix}0 & \mathbf{e}_j^T\end{bmatrix}\begin{bmatrix}\delta\\ \omega\end{bmatrix}$$

Error! Bookmark not defined.

where the notation $\mathbf{e}_{j,i}$ represents a 0-1 indicator vector (with length n) with jth entry equal to 1, ith entry equal to -1, and the others equal to 0. In addition, the notation $\mathbf{e}_q$ represents a 0-1 indicator vector (with length n) with qth entry equal to 1 and the others equal to 0.

In practice, measurement delay may arise in HVDC line compensators, since they use remote measurements to govern the line power flow. In order to study the impact of the delay on the presence or absence of nonminimum-phase dynamics, the existing dynamic model is updated to represent the delay. For this initial effort, (1,0)-Pade (1,1)-Pade approximations for the delay are used in the transfer-function analysis.

3.3. Algebraic, Structural, and Graph-Theoretic Results

The main purpose of this section is to develop structural and graph-theoretic characterizations of the input-output swing-dynamics models, for both the nominal model and the enhanced models with HVDC line controllers. The single-input single-output models considered here are fully characterized by their transfer functions, or equivalently their poles and zeros. The poles are intrinsic properties of the state dynamics of the swing models (specifically, the eigenvalues or modes of the state matrix), and do not depend on the input and output locations. These modal dynamics have been very extensively characterized in the power literature, including from a graph-theoretic perspective, and provide basic insight into the power network's small-signal dynamics. However, control design and disturbance analysis for dynamical systems crucially depend on the (finite) zeros of the transfer function, which are functions of the input-output channel in addition to the state dynamics. The importance of the zeros to control design and analysis stems from the fact that they are invariant to feedback, and hence that their locations place fundamental limits on control performance. Particularly, control performance is distinguished by the presence and absence of right half plane (nonminimum phase) zeros. Thus, as wide-area control of the power

transmission networks becomes increasingly feasible, and the networks are subject to increasing variability and disruption, characterizing the zeros of the swing-dynamics model is increasingly important. Analyses of input-output properties of the swing dynamics, including particularly the zeros, is rather sparse. Numerical computation of the zeros for the classical model has been addressed by N. Martins and co-workers (see [23]) but few structural results are available, and the influence of dynamical components (e.g., HVDC line controllers, VSCs, etc) on the zeros is not well understood.

The graph-theoretic analyses of zeros developed here are based on an algebraic transformation of linear systems known as the *special coordinate basis*. The special coordinate basis involves input, state, and output transformations of a linear system, which exposes its finite- and infinite- zero structures ([24]). Specifically, the special coordinate basis separates a linear dynamics into integrator chains from inputs to outputs (which specify the infinite-zero structure), and a *zero dynamics* connected in feedback which captures the finite zero structure. Importantly, the transformation thus enables computation of the zeros as the eigenvalues of the *state matrix of the zero dynamics*. This zeros state matrix turns out to equal a sparse perturbation of a submatrix of the system's state matrix, where the nonzero entry locations in the perturbation are tied to the network's graph.

3.3.1 Developing the Special Coordinate Basis Transformation for the Nominal Model

As a preliminary step, the relative degree of the transfer function is determined. Specifically, the following theorem shows that the relative degree is entirely governed by the distance d between the input and output, which is defined as the minimum number of directed arcs from the input to the output locations in the network graph Γ:

Theorem 1: *The relative degree of the input-output swing-dynamics model, and hence the number of infinite zeros, is* $n_d=2d+1$. *The number of finite zeros is* $n_a=2n-2d-1$.

The number of infinite zeros, which equals the relative degree, indicates the number of diverging branches on the positive root locus of the transfer function. From the classical control theory, the infinite-zero structure of a system guides controller architecture selection and control design. Theorem 1 shows that this number is entirely decided by the distance between the input and output in the graph, for the swing-dynamics model.

On the other hand, the locations of a system's finite zeros in the complex plane dictate dynamical-response characteristics (e.g., undershoot), and place essential limits on control (see Schrader (1989)). This motivates structural and graph-theoretic analysis of the finite zero locations for the swing model, in terms of its parameters and the input and output locations. As a stepping stone toward these structural analyses, first an algebraic expression for the zero state matrix is obtained. The eigenvalues of this matrix, which we denote A_{aa}, exactly specify the $2n-(2d+1)$ finite zeros of the model. The algebraic expression for A_{aa} follows from the SCB transformation of the swing-dynamics model. As Theorem 1 makes clear, the infinite zeros are essentially tied to the shortest path between the input and output vertices in Γ. We find it convenient to define some notation related to this path. In particular, we choose a path of minimum length (least number of edges)

between the input and output, and refer to it as the *special input-output path*. In addition, the nodes in the network corresponding to the vertices on the special input-output path are referred to as the nodes associated with the special input-output path. Likewise, the state variables (angle, frequency) at these nodes or buses are referred to as the state variables associated with the special input-output path, and the rows and columns of the state matrix corresponding to these state variables are also referred to as being associated with the special input-output path. Corresponding terminology is used to refer to the vertices, nodes, state variables, and matrix entries that are not on the special input-output path.

From here on, we assume (without loss of generality) a particular ordering of the original state vector and the corresponding graph vertices. Specifically, the input location in Γ is labeled as vertex n, and hence the corresponding state variables are δ_n and ω_n. Also, the

d+1 vertices along the special input-output path are labeled as follows: the vertex at a distance k from the output along the special input-output path is labeled as vertex $i=n-k$ (k=1,2,...,d). The states corresponding to each vertex are δ_{n-k} and ω_{n-k}. Hence, the input location is at vertex $i=n-d$. The remaining vertices, which are not on the special input-output path, are labeled i=1,...,$n-d-1$. For this labeling of the vertices, the state space form of the swing-dynamics model becomes:

$$\dot{\mathbf{x}} = A\mathbf{x} + (\mathbf{e}_i \otimes \begin{bmatrix}0\\1\end{bmatrix})u \tag{3}$$

$$y = (\mathbf{e}_j \otimes \begin{bmatrix}0\\1\end{bmatrix})^T \mathbf{x}, \tag{4}$$

where

$$A = \tilde{L} \otimes \begin{bmatrix}0 & 0\\1 & 0\end{bmatrix} + \tilde{D} \otimes \begin{bmatrix}0 & 0\\0 & 1\end{bmatrix} + I \otimes \begin{bmatrix}0 & 1\\0 & 0\end{bmatrix}, \tag{5}$$

and where $\tilde{L}=-H^{-1}L$ and $\tilde{D}=-H^{-1}D$. The matrix A can also be naturally partitioned as

$$A = \begin{bmatrix} A_{n_a} & A_{n_{ad}} \\ A_{n_{da}} & A_{n_d} \end{bmatrix}$$

where A_{n_a} is a matrix of dimension $(2n-(2d+1))\times(2n-(2d+1))$. We note that rows and columns of A_{n_a} are associated with the vertices (and corresponding state variables) that are not on the special input output, and in addition the angle variable associated with the input vertex. The algebraic expression for the state matrix A_{aa} of the zero dynamics is presented in the following theorem:

Theorem 2: *The finite zeros of the swing-dynamics model are the eigenvalues of matrix* $A_{aa}=A_{n_a}-A_{n_{ad}}Z_{n_d}^{-1}Z_{n_{ad}}$, *where* A_{n_a} *and* $A_{n_{ad}}$ *are submatrices of A as defined above, where*

$$Z_{n_{ad}} = \begin{bmatrix} 0 & 0 & 0 & 0 \\ \{A\}_{n_a+1,1} & \{A\}_{n_a+1,2} & \cdots & \{A\}_{n_a+1,n_a} \\ \{A^2\}_{n_a+1,1} & \{A^2\}_{n_a+1,2} & \cdots & \{A^2\}_{n_a+1,n_a} \\ \vdots & \vdots & \cdots & \vdots \\ \{A^{n_d-1}\}_{n_a+1,1} & \{A^{n_d-1}\}_{n_a+1,2} & \cdots & \{A^{n_d-1}\}_{n_a+1,n_a} \end{bmatrix} \quad (6)$$

and where Z_{n_d} is the following lower triangular matrix:

$$Z_{n_d} = \begin{bmatrix} 1 & 0 & \cdots & 0 \\ \{A\}_{n_a+1,n_a+1} & \{A\}_{n_a+1,n_a+2} & \cdots & 0 \\ \vdots & \vdots & \ddots & \\ \{A^{n_d-1}\}_{n_a+1,n_a+1} & \{A^{n_d-1}\}_{n_a+1,n_a+2} & \cdots & 0 \\ & & & \{A^{n_d-1}\}_{n_a+1,2n} \end{bmatrix} \quad (7)$$

Remark: The matrix $Z_{n_d}^{-1}$ is a lower triangular matrix. An iterative formula for its entries can be developed in a similar fashion to the analysis in [12,13]. This computation is omitted to save space.

The algebraic expression for the zero state matrix A_{aa} in Theorem 2 enables the development of structural and graph-theoretic insights. To develop these results, it is useful to recognize that A_{aa} is in the form $A_{aa}=A_{n_a}+A_q$, where A_{n_a} is a principal submatrix of the state matrix A and A_q is a perturbation matrix which has a special sparse structure.

The following theorem gives the main structural insight:

Theorem 3: The matrix A_{aa}, whose eigenvalues are the zeros of the swing-dynamics model, can be expressed in the form $A_{aa}=A_{n_a}+A_q$. Let us define $[A_{aa}]_{i,j}$ (respectively $[A_{n_a}]_{i,j}$) to refer to the 2×2 submatrix of A_{aa} (respectively A_{n_a}) whose rows are associated with vertex i, and whose columns are associated with vertex j. Also, let d_i be the distance from the input location to the vertex i in Γ, and let d_j be the distance from vertex j to the output location in Γ. We have that $[A_{aa}]_{i,j}=[A_{n_a}]_{i,j}$, unless $d_i+d_j \leq d+1$ and i is adjacent to a vertex in the special input-output path other than the output. For $d_i+d_j \leq d+1$, $[A_{aa}]_{i,j}$ may differ from $[A_{n_a}]_{i,j}$. However, the row of $[A_{aa}]_{i,j}$ corresponding to δ_i is equal to this row of $[A_{n_a}]_{i,j}$ (these entries in the perturbation are always 0). Also, the entry of $[A_{aa}]_{i,j}$ corresponding to ω_i and ω_j differs from this entry for $A_{n_a i,j}$ only if $d_i+d_j \leq d$.

Theorem 3 expresses that the matrix A_{aa} can be viewed as a perturbation of the principal submatrix A_{n_a} of A associated with the vertices that are not on the special input-output path. Since this is the case, we also identify the rows and columns of A_{aa} by their associated vertices in the graph Γ, specifically the vertices off the special input-output path whose state variables correspond to these rows and columns. The main outcome of Theorem 3 is that the perturbation A_q is structured, in the sense only certain entries of A_{aa} differ from those of A_{n_a} based on the network graph Γ. Specifically, consider an entry in A_q whose row corresponds to vertex i and whose column corresponds to vertex j (where i and j are not on the special input-output path). The entry can be non-zero only if the distance of j from the output in Γ plus the distance of i from the input in Γ is at most d+1 (the length of the special input-output path plus 1). Additionally, the vertex i must be adjacent to the special input-output path. Thus, only the entries whose rows and columns correspond to vertices near the input-output path are perturbed.

Remark: Finding the zeros by computing A_{aa} and then finding its eigenvalues is also attractive from a computational standpoint.

3.3.2. Graph-Theoretic Analyses of the Nominal Model

In this subsection, several conditions for minimum-phase dynamics are presented for the nominal model without HVDC. As mentioned in previous subsection, expressing the matrix A_{aa} as a perturbation of A_{n_a} enables graph-theoretic analysis of the zeros, as developed in the following theorems. These analyses require first noting that the eigenvalues of the matrix A_{n_a} are in the closed left half plane. Precisely, the matrix A_{n_a} has a single eigenvalue at s=0 (associated with the angle dynamics of the input bus), and the remaining eigenvalues are strictly in the OLHP. Since the matrix A_{n_a} is stable, the eigenvalues of the matrix A_{aa} and hence the zeros of the swing models can be guaranteed to be in the left half plane if the perturbation A_q either does not change the eigenvalues of A_{n_a}, or is sufficiently small. The following theorems use this idea to give structural conditions under which the swing-dynamics model is minimum phase.
The first of these structural results addresses the case that the input and output are at the same vertex in Γ (the same bus in the network):

Theorem 4: *The input-output swing-dynamics model has all zeros in the OLHP, except one zero at s=0, if the input and output locations are at the same vertex.*

The second of these structural results addresses the case that there is only a single path between the input and output:

Theorem 5: *The input-output swing-dynamics model has all zeros in the OLHP, except one zero at s=0, if there is a single path between the input and output vertices in the network graph Γ.*

The next result shows that minimum-phase dynamics are maintained even when there are multiple paths between the input and output, provided that the special input-output path is sufficiently strong (has high susceptances) compared to the other paths.

Theorem 6: *Consider the zeros of the input-output swing-dynamics model for an arbitrary graph Γ. Now consider scaling up all the edge weights on a special input-output path by a factor κ. For sufficiently κ, the zeros are in the OLHP except one zero at $s=0$.*

Conversely, the swing-dynamics model is nonminimum-phase if the special input-output path is sufficiently weak compared to other longer paths between the input and output. A proof of the nonminimum-phase result is rather involved, see Abad Torres (2015) for a similar proof for a simpler synchronization model.

The graph-theoretic analysis of zeros developed here can potentially support power-system analysis and controller design in several ways. First, the results give insight into estimation and control of the dynamics. It is well known that the finite and infinite zero structure of a system, and particularly the presence of nonminimum-phase zeros, place essential limits on estimator and control performance and guide control design. For instance, for control channels, the locations of zeros determine whether or not high-gain control is viable and place restrictions on reference tracking and disturbance rejection. Likewise, the zeros of a disturbance-input-to-sensor transfer function influence whether or not dynamic state filtering is possible in the presence of unknown disturbance inputs. In current power-grid operations, control designs are often simplistic in nature, perhaps using simple proportional-integral-derivative controllers with manually-tuned parameters. Our work shows that the network's topology modulates whether such simple control schemes are likely to work or fail. Specifically, if the input and output are collocated, or the shortest path between then is the dominant one, then the channel of interest is minimum-phase and simple control/filtering algorithms may be apt. On the other hand, if the network has alternate long paths between the input and output, caution is needed to ensure that the dynamics is indeed minimum phase, and more sophisticated designs are needed if it is not. This intuition further leads to shortest-path-type algorithms for screening for non-minimum-phase channels, and for placing sensors or actuators to avoid nonminimum-phase characteristics. Details are omitted in the interest of space.

In addition, let us continue the conditions for minimum-phase dynamics by three theorems. Two of these results specify how generator inertia and damping impact zero locations. The third result studies whether interconnections of two networks are minimum-phase. These conditions are important for assessment and design of small-signal characteristics of the power transmission network, because they identify network properties and input-output channels that guarantee minimum-phase behaviors, over a range of operating conditions. Here is the next result:

Theorem 7: *Consider the zeros of the input-output swing dynamics model for an arbitrary graph Γ. The zeros have no dependence on the damping and inertia of generators at the input and output vertices.*

Theorem 7 shows that, surprisingly, the damping and inertia of the generators at the input and output locations do not affect the zeros. Thus, while local changes in generator models can change

zeros for remote input-output channels, they do not alter the zero properties for channels whose input or output are at the location of the change.

The next result considers the interconnection of minimum-phase networks via a single line. The result generalizes a preliminary result obtained in Theorem 5, which states that all zeros of the input-output dynamics are in the OLHP (except one at s=0) if there is a single path between the input and output vertices in the network graph Γ, Power networks typically do not entirely have a tree structure, hence this condition is not directly applicable, however it is more typical that the transmission network comprises strongly-interconnected pieces with single lines (or a sparse set of lines) between them. The following result gives insight into the swing dynamics for networks with this structure:

Theorem 8: *Consider the input-output swing dynamics in the case that the network graph Γ can be partitioned into subgraphs Γ_1 and Γ_2, such that: 1) Γ_1 contains the input i, 2) Γ_2 contains the output j, and 3) there is only a single edge between Γ_1 and Γ_2 (in other words, the network graph has a single edge cut separating the input and output). The ends of the edge connecting Γ_1 and Γ_2 are labeled n_{c1} and n_{c2}, respectively. Now consider two swing dynamics models for the subnetworks defined on Γ_1 and Γ_2*

1. *System S_1: Input-output swing dynamics model with input at vertex i and output at vertex n_{c1}, for the subnetwork defined on graph Γ_1.*

2. *System S_2: Input-output swing dynamics model with input at vertex n_{c2} and output at vertex j, for the subnetwork defined on graph Γ_2.*

The zeros of the full input-output swing-dynamics model defined on Γ are the union of: 1) the zeros of S_1, 2) the zeros of S_2, and 3) possibly a subset of the (stable) poles of S_1 and S_2.

Theorem 8 shows that the interconnection of two networks with minimum-phase swing dynamics by a single line yields a full network that is also minimum phase. In fact, the swing dynamics for the interconnected network precisely preserves the zeros of the individual networks. The result gives insight into inter-area swings in the bulk power grid. Specifically, the result indicates that, for a network with two areas connected by a single line, guaranteeing minimum-phase transfer functions for each area also guarantees minimum-phase transfer functions across the areas. On the other hand, the presence of multiple paths for power flow between the areas can introduce nonminimum-phase dynamics.

The following result characterizes the impact of generator dampings on the zero locations. Intuition suggests that well-damped networks should be less susceptible to oscillations, hence input-output channels should be minimum phase. The following result verifies that this is the case, for a broad class of swing-dynamics models. The result builds on several results developed previously, which show that the shortest path in Γ between the input and output (called the special

input-output path) determine the structure of the special coordinate basis, and hence whether or not the system is minimum phase. Here is the result regarding dampings:

Theorem 9 *Consider the zeros of the input-output swing dynamics model, in the case that the network graph Γ has only one minimum-length path between the input and output vertices. (Note that the graph may have an arbitrary number of paths between input and output, but the path of minimum length should be unique.) Now consider scaling up the damping of all generators by a factor κ. For sufficiently large κ, the zeros are in the OLHP except one zero at s=0.*

Theorem 9 shows that input-output channels in the power transmission network are minimum phase provided that the network is sufficiently damped (under the technical assumption that the minimum-length path between the input and output is unique). We conjecture that the result in fact holds for arbitrary networks: however, the proof becomes more intricate when there is more than one minimum-length path between the input and output.

3.3.3. Analysis of Networks with Controlled HVDC Lines

Graph-theoretic results on the zeros of the swing-dynamics model are developed, for the case where controlled HVDC lines are present in the transmission network. Modern power transmission networks commonly include HVDC lines for stability and cost purposes. It is important to understand whether the integration of HVDC lines, and particularly the controls used on these lines, influence input-output behaviors in a power transmission network. In general, addition of an HVDC line may alter input-output channel properties throughout the network. As a first step, we study how the control on the HVDC line impacts the transfer function across the line (i.e., the transfer function when the input is the power injection on one end of the line, and the output is the frequency at the other end). This case is of particular interest because it gives insight into whether or not addition of an HVDC line between two buses improves the transfer characteristics for this channel, and also indicates the susceptibility of the HVDC control to disruption. In the following three theorems, we discuss the effect of HVDC line on zeros for different controllers applied across the line, focusing on specifying conditions that guarantee minimum-phase dynamics.

Theorem 10: *Consider the input-output swing dynamics model, in the case that there is a proportional-controlled HVDC line between the input and the output buses. If a sufficiently large proportional gain k is used on the HVDC line, the zeros of the system are in the OLHP except one zero at s=0.*

Theorem 11: *Consider the input-output swing-dynamics model, with PD-controlled HVDC line between the input and the output vertices. If either the derivative gain k_d or the proportional gain k_p is large enough, the zeros of the model are in the OLHP except one zero at s=0.*

Theorem 12: *Consider the input-output swing dynamics model, with a lead-compensated HVDC line between the input and output (specifically, a compensator of the form* $P_{i,o}=k\frac{1+T_1 s}{1+T_2 s}(\delta_i-\delta_o)$

). If the product kT_1 is sufficiently large (i.e. either k or T_1 is sufficiently large) and T_2 is sufficiently small, the zeros of the system are in the OLHP except one zero at s=0.

The impact of an HVDC line with strong control on other channels in the networks, where the input and output are not the ends of the HVDC, is also of significant interest. Since the HVDC line in this case can make alternative long paths from the input to the output strong, there is a possibility that the HVDC modulation may cause other channels to become nonminimum phase. A formal study of this impact will be undertaken in further work.

In practice, HVDC line controllers may be subject to measurement delay, since they use remote measurements to govern the line power flow. In the next theorems, we study the impact of the delay on the presence or absence of nonminimum-phase dynamics, using (1,0) and (1,1) Pade approximations for the delay in the transfer-function analysis. The main outcome of this analysis is show that proportional and lag compensation schemes with sufficient gain yield nonminimum-phase transfer functions, if measurement delays are present.

Theorem 13: *Consider the input-output swing-dynamics model with proportional-controlled HVDC line between input and output, where the controller is subject to a measurement delay T_1. The compensator with delay can be approximated as $P_{i,o}=k(1-T_1 s)(\delta_i-\delta_o)$, where a (1,0) Pade approximation has been used for the delay. If the proportional gain k of the HVDC line is sufficiently large, one of the zeros of the system will be in the ORHP, i.e. the system will be non-minimum phase.*

Theorem 14: *Consider the input-output swing-dynamics model with proportional-controlled HVDC line between input and output, where the controller is subject to a measurement delay T_d. The compensator with delay can be approximated as $P_{i,o}=k\frac{(1-0.5T_d s)}{(1+0.5T_d s)}(\delta_i-\delta_o)$, where a (1,1)-Pade approximation has been used for the delay. If the proportional gain k of the HVDC line is sufficiently large and delay T_d is sufficiently small, one of the zeros of the system will be in the ORHP, i.e. the system will be non-minimum phase.*

Theorem 15: *Consider the input-output swing dynamics model with lag-controlled HVDC line between input and output, where the controller is subject to a measurement delay T_d. The compensator with delay can be approximated as $P_{i,o}=k\frac{1-T_d s}{1+T_2 s}(\delta_i-\delta_o)$, where the (1,0) Pade approximation has been used for the delay. If kT_d is sufficiently large (i.e. either k or T_d are sufficiently large), and T_2 is sufficiently small, one of zeros of the system will be in the ORHP, so the system is non-minimum phase.*

While the analyses here are based on the Pade approximation, we hypothesize that the results carry through to an exact model of the delay. We expect to pursue this analysis in further work.

4. Analysis of Zeros in Detailed Power-System Models

The pioneering work by Martins et.al. in [23] proposed methods for studying transfer function zeroes in large-scale power system models. Recent advances in wide-area monitoring technology using synchrophasors have led to renewed interest in the design of wide-area controls that are based on remote input signals for addressing advanced stability control issues. In Section 2, it has been shown using the classical model that such wide-area control designs can sometimes lead to nonminimum phase zeroes that complicate the closed loop control design and performance. Specifically, analytical conditions were developed for when such right half plane (RHP) zeros can appear in general power system dynamics represented by classical angle stability models using swing equations. In this section, as a complementary effort, we will study the presence and impact of RHP transfer function zeros in detailed power system models of test power systems. In this initial effort on detailed models, we present results for the 11 bus Kundur test power system. The zeros are calculated using the linearized state matrices from the commercial program Small-Signal Analysis Tool (SSAT) developed by Powertech Labs Inc., Vancouver, BC, Canada.

4.1. Results on Zero Locations

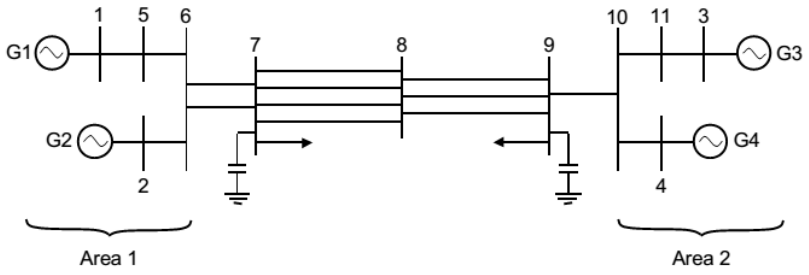

Figure 5: Two-area Kundur test system [25].

Let us consider the two-area test system from [25]. This system is commonly used for studying inter-area oscillations. Under high power transfers, it can be shown that the system has a poorly damped inter-area mode [25]. For instance, traditional power system stabilizer (PSS) designs using local generator signals are discussed in [25] for improving the damping of this inter-area mode. In our case, we are interested in the design of power system stabilizers using remote input signals. Suppose we consider the PSS design for generator 1 using remote input signals. Then, the exciter control voltage reference Vref is set to be the input while the output is assumed to be from three choices of signals:

a) Machine speed measurements at one of the four generators 1, 2, 3 and 4,
b) Bus voltage magnitude measurements at any of the 11 buses in Figure 1, and
c) Phase angle differences between specific bus voltage phasors in Figure 1. Machine speed measurement (or bus frequency measurement) at generator 1 would be a traditional input choice for the PSS design for generator 1.

4.1.1. Machine speed input signals

Table 1 shows the zeros of pairs of input V_{ref1} and the generators speed as outputs. It is interesting that there are no RHP zeros for the traditional PSS design while using generator 1 speed as the output. If any other generator speed is used as the output for the transfer function (which would then be the input for the generator 1 PSS design), the transfer function has RHP zeros some real and some complex conjugate.

ω_1	ω_2	ω_3	ω_4
Inf + 0.0000i	Inf + 0.0000i	Inf + 0.0000i	Inf + 0.0000i
Inf + 0.0000i	-25.0000 + 0.0000i	-25.0000 + 0.0000i	-25.0000 + 0.0000i
Inf + 0.0000i	-25.0000 + 0.0000i	-25.0000 + 0.0000i	-25.0000 + 0.0000i
-66.6667 + 0.0000i	-0.5000 + 0.0000i	-0.5000 + 0.0000i	-0.5000 + 0.0000i
-52.8418 + 0.0000i	Inf + 0.0000i	Inf + 0.0000i	Inf + 0.0000i
-51.8304 + 0.0000i	-66.6667 + 0.0000i	-66.6667 + 0.0000i	-66.6667 + 0.0000i
-52.3616 + 0.0000i	-53.5764 + 0.0000i	-1.6922 +28.8549i	-53.9529 + 0.0000i
-37.2769 + 0.0000i	-52.7314 + 0.0000i	-1.6922 -28.8549i	-52.1882 + 0.0000i
-35.4649 + 0.0000i	-51.8311 + 0.0000i	-54.2339 + 0.0000i	-51.3935 + 0.0000i
-33.3004 + 0.0000i	-13.5517 +17.4020i	-51.4552 + 0.2407i	-9.0535 +23.3958i
-32.7030 + 0.0000i	-13.5517 -17.4020i	-51.4552 - 0.2407i	-9.0535 -23.3958i
-31.5697 + 0.0000i	-37.2681 + 0.0000i	9.1736 + 0.0000i	-38.7652 + 0.0000i
-29.3369 + 0.0000i	-34.5507 + 0.0000i	-38.7995 + 0.2745i	7.0961 + 0.0000i
-28.7531 + 0.0000i	-32.9208 + 0.2752i	-38.7995 - 0.2745i	-35.8529 + 0.0000i
-14.3792 + 8.8796i	-32.9208 - 0.2752i	-33.5363 + 0.0000i	-33.8332 + 0.0000i
-14.3792 - 8.8796i	-30.8328 + 0.0000i	-32.4726 + 0.0000i	-32.8629 + 0.0000i
-22.4634 + 4.4317i	-28.7522 + 0.0000i	-30.2540 + 0.0000i	-30.4902 + 0.0000i
-22.4634 - 4.4317i	-15.5660 + 7.3489i	-28.7792 + 0.0000i	-28.7643 + 0.0000i
-20.5594 + 4.2457i	-15.5660 - 7.3489i	-23.1699 + 4.7756i	-22.9930 + 4.2639i
-20.5594 - 4.2457i	-22.4629 + 4.4328i	-23.1699 - 4.7756i	-22.9930 - 4.2639i
-20.8718 + 0.0000i	-22.4629 - 4.4328i	-22.8781 + 3.9116i	-21.4286 + 4.4106i
-0.7872 + 7.4941i	-20.4760+ 0.0000i	-22.8781 - 3.9116i	-21.4286 - 4.4106i
-0.7872 - 7.4941i	3.9602 + 0.0000i	-1.0550 + 8.6825i	-0.9235 + 8.0751i
-0.6169 + 5.0700i	-0.7869 + 7.4919i	-1.0550 - 8.6825i	-0.9235 - 8.0751i
-0.6169 - 5.0700i	-0.7869 - 7.4919i	-0.8265 + 7.9500i	-0.6508 + 6.6964i
-10.3045+0.0000i	0.1449 + 3.9105i	-0.8265 - 7.9500i	-0.6508 - 6.6964i
-8.7583 + 0.0000i	0.1449 - 3.9105i	-8.5776 + 0.3811i	-10.7208+ 0.0000i
-0.7951 + 1.3990i	-7.0016 + 0.0000i	-8.5776 - 0.3811i	-8.2054 + 0.0000i
-0.7951 - 1.3990i	-8.7209 + 0.0000i	-6.1039 + 0.0000i	-6.3511 + 0.0000i
-4.3255 + 0.0646i	-1.3034 + 0.0000i	-3.4058 + 0.0000i	-3.4105 + 0.0000i
-4.3255 - 0.0646i	-3.3566 + 0.0000i	-1.6977 + 0.0000i	-3.0164 + 0.0000i
-3.1854 + 0.0000i	-3.4950 + 0.0000i	-2.5953 + 0.0867i	-1.6842 + 0.0000i
-2.3987 + 0.0000i	-2.3819 + 0.0000i	-2.5953 - 0.0867i	-2.2213 + 0.0000i
-0.5699 + 0.0000i	-0.4956 + 0.0000i	-0.5155 + 0.0000i	-0.5155 + 0.0000i
-0.5070 + 0.0000i	-0.5094 + 0.0000i	-0.5101 + 0.0000i	-0.5089 + 0.0000i

-0.5096 + 0.0000i	Inf + 0.0000i	Inf + 0.0000i	Inf + 0.0000i
Inf + 0.0000i	Inf + 0.0000i	Inf + 0.0000i	Inf + 0.0000i
Inf + 0.0000i	Inf + 0.0000i	Inf + 0.0000i	Inf + 0.0000i
Inf + 0.0000i	Inf + 0.0000i	Inf + 0.0000i	Inf + 0.0000i
Inf + 0.0000i	Inf + 0.0000i	Inf + 0.0000i	Inf + 0.0000i
Inf + 0.0000i	Inf + 0.0000i	Inf + 0.0000i	Inf + 0.0000i
Inf + 0.0000i	Inf + 0.0000i	Inf + 0.0000i	Inf + 0.0000i
Inf + 0.0000i	Inf + 0.0000i	Inf + 0.0000i	Inf + 0.0000i
Inf + 0.0000i	Inf + 0.0000i	Inf + 0.0000i	Inf + 0.0000i
Inf + 0.0000i	Inf + 0.0000i	Inf + 0.0000i	Inf + 0.0000i
Inf + 0.0000i	Inf + 0.0000i	Inf + 0.0000i	Inf + 0.0000i
Inf + 0.0000i	Inf + 0.0000i	Inf + 0.0000i	Inf + 0.0000i
Inf + 0.0000i	Inf + 0.0000i	Inf + 0.0000i	Inf + 0.0000i
Inf + 0.0000i	Inf + 0.0000i	Inf + 0.0000i	Inf + 0.0000i
Inf + 0.0000i	Inf + 0.0000i	Inf + 0.0000i	Inf + 0.0000i
Inf + 0.0000i	Inf + 0.0000i	Inf + 0.0000i	Inf + 0.0000i
Inf + 0.0000i	Inf + 0.0000i	Inf + 0.0000i	Inf + 0.0000i
Inf + 0.0000i	Inf + 0.0000i	Inf + 0.0000i	Inf + 0.0000i
Inf + 0.0000i	Inf + 0.0000i	Inf + 0.0000i	Inf + 0.0000i
Inf + 0.0000i	Inf + 0.0000i	Inf + 0.0000i	Inf + 0.0000i
Inf + 0.0000i	Inf + 0.0000i	Inf + 0.0000i	Inf + 0.0000i
Inf + 0.0000i	Inf + 0.0000i	Inf + 0.0000i	Inf + 0.0000i
Inf + 0.0000i	Inf + 0.0000i	Inf + 0.0000i	Inf + 0.0000i
Inf + 0.0000i	Inf + 0.0000i	Inf + 0.0000i	Inf + 0.0000i
0.0000 + 0.0000i	0.0000 + 0.0000i	0.0000 + 0.0000i	0.0000 + 0.0000i
-25.0000 + 0.0000i	-25.0000 + 0.0000i	-25.0000 + 0.0000i	-25.0000 + 0.0000i
-25.0000 + 0.0000i	-25.0000 + 0.0000i	-25.0000 + 0.0000i	-25.0000 + 0.0000i
-0.5000 + 0.0000i	-0.5000 + 0.0000i	-0.5000 + 0.0000i	-0.5000 + 0.0000i
Inf + 0.0000i	Inf + 0.0000i	Inf + 0.0000i	Inf + 0.0000i

Table 1: Transfer function zeros for input V_{ref1} paired with different generators speed output.

4.1.2. Bus voltage magnitude input signals

Tables 2 and 3 show the zeros of the input V_{ref1} paired with different bus voltage magnitudes as outputs. In this case, the transfer function has one real RHP zero for each choice of voltage magnitude signals V1 through V11.

Bus 1	Bus 2	Bus 3	Bus 4	Bus 5
-25.0000 + 0.0000i	-25.0000 + 0.0000i	-25.0000 + 0.0000i	-25.0000 + 0.0000i	-25.0000 + 0.0000i
-25.0000 + 0.0000i	-25.0000 + 0.0000i	-25.0000 + 0.0000i	-25.0000 + 0.0000i	-25.0000 + 0.0000i
-0.5000 + 0.0000i	-0.5000 + 0.0000i	-0.5000 + 0.0000i	-0.5000 + 0.0000i	-0.5000 + 0.0000i
-66.6667 + 0.0000i	-66.6667 + 0.0000i	-66.6667 + 0.0000i	-66.6667 + 0.0000i	-66.6667 + 0.0000i
-52.8153 + 0.0000i	-52.7690 + 0.0000i	-51.3867 + 0.1681i	-52.1541 + 0.0000i	-52.7947 + 0.0000i
-52.1488 + 0.0000i	-51.8323 + 0.0000i	-51.3867 - 0.1681i	-51.3494 + 0.0000i	-51.9768 + 0.0000i
-51.8285 + 0.0000i	-47.4020 + 0.0000i	-47.9107 + 0.0000i	-47.2889 + 0.0000i	-51.8272 + 0.0000i
-37.2748 + 0.0000i	-45.4771 + 0.0000i	-44.8286 + 0.0000i	-45.6106 + 0.0000i	-37.2663 + 0.0000i
-36.6792 + 0.0000i	-37.2641 + 0.0000i	-38.7897 + 0.3091i	-38.7456 + 0.0000i	-36.9847 + 0.0000i
-33.2894 + 0.0000i	-34.9181 + 0.0000i	-38.7897 - 0.3091i	-35.9591 + 0.0000i	-33.3439 + 0.0000i
-32.7196 + 0.0000i	-32.9320 + 0.2601i	-33.5176 + 0.0000i	-33.9146 + 0.0000i	-32.6262 + 0.0000i
-31.6973 + 0.0000i	-32.9320 - 0.2601i	-32.4066 + 0.0000i	-32.8903 + 0.0000i	-32.1291 + 0.0000i
-29.9395 + 0.0000i	-30.6296 + 0.0000i	-28.6996 + 0.0000i	-29.4600 + 0.0000i	-30.1815 + 0.0000i
-28.7515 + 0.0000i	-28.7515 + 0.0000i	-27.6856 + 3.1709i	-28.7987 + 0.0000i	-28.7516 + 0.0000i
-14.6125 + 8.7972i	-15.0875 + 8.0248i	-27.6856 - 3.1709i	-24.5562 + 3.6469i	-14.7686 + 8.5226i
-14.6125 - 8.7972i	-15.0875 - 8.0248i	-25.4815 + 0.0000i	-24.5562 - 3.6469i	-14.7686 - 8.5226i
-22.4680 + 4.4310i	-23.7720 + 3.8650i	-23.2894 + 4.0893i	-23.1890 + 4.0776i	-21.8842 + 4.5218i
-22.4680 - 4.4310i	-23.7720 - 3.8650i	-23.2894 - 4.0893i	-23.1890 - 4.0776i	-21.8842 - 4.5218i
-21.3839 + 4.4930i	-22.4582 + 4.4343i	-22.9391 + 4.2468i	-21.8809 + 4.4484i	-22.4724 + 4.4298i
-21.3839 - 4.4930i	-22.4582 - 4.4343i	-22.9391 - 4.2468i	-21.8809 - 4.4484i	-22.4724 - 4.4298i
-20.8928 + 0.0000i	-20.6929 + 0.0000i	-0.4178 + 8.0458i	-0.4252 + 7.9072i	-20.8136 + 0.0000i
-0.9315 + 7.3888i	-0.3336 + 7.8855i	-0.4178 - 8.0458i	-0.4252 - 7.9072i	-0.8037 + 7.6521i
-0.9315 - 7.3888i	-0.3336 - 7.8855i	-0.8854 + 7.7258i	-0.8145 + 7.7218i	-0.8037 - 7.6521i
-0.7834 + 7.5088i	-0.8063 + 7.4948i	-0.8854 - 7.7258i	-0.8145 - 7.7218i	-0.8125 + 7.5035i
-0.7834 - 7.5088i	-0.8063 - 7.4948i	-0.2670 + 5.1801i	-0.2829 + 5.0241i	-0.8125 - 7.5035i
-0.1359 + 4.4397i	-0.1568 + 4.7811i	-0.2670 - 5.1801i	-0.2829 - 5.0241i	-0.1556 + 4.5606i

-0.1359 - 4.4397i	-0.1568 - 4.7811i	2.8672 + 0.0000i	-10.2811 + 0.0000i	-0.1556 - 4.5606i
-10.0631 + 0.0000i	-8.7335 + 0.0000i	-8.0255 + 0.4592i	-7.9010 + 0.0000i	-9.2210 + 0.0000i
-8.7294 + 0.0000i	-6.4548 + 0.0000i	-8.0255 - 0.4592i	-6.1744 + 0.0000i	-8.7298 + 0.0000i
-3.4635 + 0.2023i	-3.4097 + 0.0960i	-6.0490 + 0.0000i	1.9695 + 0.0000i	-3.4303 + 0.1649i
-3.4635 - 0.2023i	-3.4097 - 0.0960i	-3.3646 + 0.0000i	-3.3582 + 0.0000i	-3.4303 - 0.1649i
-2.9458 + 0.0000i	-2.3885 + 0.0000i	-2.1026 + 0.3799i	-1.8754 + 0.0000i	-2.6994 + 0.0000i
-2.3869 + 0.0000i	-1.0374 + 0.0000i	-2.1026 - 0.3799i	-1.5520 + 0.0000i	-2.3858 + 0.0000i
-0.8268 + 0.0000i	0.3174 + 0.0000i	-1.6909 + 0.0000i	-2.7278 + 0.0000i	-0.8133 + 0.0000i
0.0831 + 0.0000i	-0.0232 + 0.0844i	-0.0086 + 0.0942i	-0.0102 + 0.0978i	0.0847 + 0.0000i
-0.0774 + 0.0000i	-0.0232 - 0.0844i	-0.0086 - 0.0942i	-0.0102 - 0.0978i	-0.0790 + 0.0000i
-0.5073 + 0.0000i	-0.4974 + 0.0000i	-0.5155 + 0.0000i	-0.5155 + 0.0000i	-0.5097 + 0.0000i
-0.5096 + 0.0000i	-0.5094 + 0.0000i	-0.5101 + 0.0000i	-0.5089 + 0.0000i	-0.5079 + 0.0000i

Table 2: Transfer function zeros with input V_{ref1} paired with different bus voltage magnitude outputs

Bus 6	Bus 7	Bus 8	Bus 9	Bus 10	Bus 11
-25.0000+0.0000i	-25.0000+0.0000i	-25.0000+0.0000i	-25.0000+0.0000i	-25.0000+0.0000i	-25.0000+0.0000i
-25.0000+0.0000i	-25.0000+0.0000i	-25.0000+0.0000i	-25.0000+0.0000i	-25.0000+0.0000i	-25.0000+0.0000i
-0.5000+0.0000i	-0.5000+0.0000i	-0.5000+0.0000i	-0.5000+0.0000i	-0.5000+0.0000i	-0.5000+0.0000i
-66.6667+0.0000i	-66.6667+0.0000i	-66.6667+0.0000i	-66.6667+0.0000i	-66.6667+0.0000i	-66.6667+0.0000i
-52.7572+0.0000i	-52.7410+0.0000i	-52.6844+0.0000i	-52.3033+0.0000i	-50.7972+0.0000i	-50.6340+0.0000i
-51.1445+0.0000i	-51.1323+0.0000i	-51.0970+0.0000i	-50.9382+0.0000i	-52.1881+0.0000i	-51.6313+0.1525i
-51.8298+0.0000i	-51.8271+0.0000i	-51.8168+0.0000i	-51.6639+0.0000i	-51.5418+0.0000i	-51.6313-0.1525i
-38.6058+0.0000i	-38.5966+0.0000i	-38.5668+0.0000i	-38.3903+0.3605i	-38.7423+0.4587i	-38.7739+0.5664i
-37.2886+0.0000i	-37.3078+0.0000i	-37.3847+0.0000i	-38.3903-0.3605i	-38.7423-0.4587i	-38.7739-0.5664i
-33.9859+0.0000i	-34.0509+0.0000i	-34.2929+0.0000i	-35.3405+0.0000i	-35.6265+0.0000i	-37.8078+0.0000i
-32.8903+0.3086i	-32.9363+0.2637i	-33.1142+0.0000i	-33.6587+0.0000i	-33.7246+0.0000i	-33.5656+0.0000i
-32.8903-0.3086i	-32.9363-0.2637i	-32.9665+0.0000i	-32.8180+0.0000i	-32.8149+0.0000i	-32.5770+0.0000i
-30.5119+0.0000i	-30.5118+0.0000i	-30.4848+0.0000i	-29.9590+0.0000i	-29.6850+0.0000i	-28.7800+0.2204i
-28.7518+0.0000i	-28.7519+0.0000i	-28.7527+0.0000i	-28.7635+0.0000i	-28.7747+0.0000i	-28.7800-0.2204i

-15.0842+7.9790i	-15.1799+7.7849i	-15.5389+7.0655i	-23.0137+4.6825i	-23.4452+4.8492i	-24.5903+4.5986i
-15.0842-7.9790i	-15.1799-7.7849i	-15.5389-7.0655i	-23.0137-4.6825i	-23.4452-4.8492i	-24.5903-4.5986i
-23.0262+4.3086i	-23.0307+4.3077i	-23.0388+4.3084i	-22.6818+4.1630i	-22.7909+3.8661i	-23.2476+3.6638i
-23.0262-4.3086i	-23.0307-4.3077i	-23.0388-4.3084i	-22.6818-4.1630i	-22.7909-3.8661i	-23.2476-3.6638i
-22.4548+4.4369i	-22.4574+4.4367i	-22.4681+4.4357i	-21.2526+4.3265i	-22.0142+4.3622i	-22.7959+4.3189i
-22.4548-4.4369i	-22.4574-4.4367i	-22.4681-4.4357i	-21.2526-4.3265i	-22.0142-4.3622i	-22.7959-4.3189i
-20.6518+0.0000i	-20.5759+0.0000i	-20.2523+0.0000i	-0.4095+7.9179i	-0.4239+7.9716i	-0.3926+8.0356i
-0.5159+7.9446i	-0.4974+7.9254i	-0.4463+7.8745i	-0.4095-7.9179i	-0.4239-7.9716i	-0.3926-8.0356i
-0.5159-7.9446i	-0.4974-7.9254i	-0.4463-7.8745i	-0.8680+7.6555i	-0.8521+7.6837i	-0.8623+7.7282i
-0.8087+7.5043i	-0.8150+7.5117i	-0.8370+7.5367i	-0.8680-7.6555i	-0.8521-7.6837i	-0.8623-7.7282i
-0.8087-7.5043i	-0.8150-7.5117i	-0.8370-7.5367i	-11.5026+0.0000i	-0.4647+4.7455i	-0.7224+4.8132i
-0.1499+4.8912i	-0.1285+5.0339i	-0.0712+5.3513i	-0.1794+5.0361i	-0.4647-4.7455i	-0.7224-4.8132i
-0.1499-4.8912i	-0.1285-5.0339i	-0.0712-5.3513i	-0.1794-5.0361i	-10.3854+0.0000i	-8.3559+0.3840i
-7.5234+0.0000i	-7.5082+0.0000i	-7.4658+0.0000i	-8.3596+0.0000i	-8.1543+0.0000i	-8.3559-0.3840i
-8.7276+0.0000i	-8.7218+0.0000i	-8.6986+0.0000i	-7.1609+0.0000i	-6.8883+0.0000i	-6.5446+0.0000i
-3.4044+0.1119i	-3.3966+0.1091i	-3.3687+0.1021i	-3.3451+0.0000i	-3.3510+0.0000i	1.7785+0.0000i
-3.4044-0.1119i	-3.3966-0.1091i	-3.3687-0.1021i	-2.8759+0.0000i	0.6875+0.0000i	-3.3590+0.0000i

-1.7791+0.0000i	-1.7765+0.0000i	-2.3813+0.0000i	-2.2345+0.0000i	-2.7006+0.0000i	-2.2098+0.2486i
-2.3884+0.0000i	-2.3872+0.0000i	-1.7702+0.0000i	-1.7409+0.0000i	-2.0789+0.0000i	-2.2098-0.2486i
-0.7087+0.0000i	0.0942+0.0000i	0.0983+0.0000i	0.2323+0.0000i	-1.7108+0.0000i	-1.6999+0.0000i
0.0932+0.0000i	-0.7041+0.0000i	-0.6796+0.0000i	-0.1520+0.1621i	-0.0352+0.1446i	-0.0125+0.1069i
-0.0881+0.0000i	-0.0890+0.0000i	-0.0932+0.0000i	-0.1520-0.1621i	-0.0352-0.1446i	-0.0125-0.1069i
-0.5152+0.0000i	-0.5152+0.0000i	-0.5152+0.0000i	-0.5156+0.0000i	-0.5155+0.0000i	-0.5155+0.0000i
-0.5092+0.0000i	-0.5092+0.0000i	-0.5092+0.0000i	-0.5092+0.0000i	-0.5092+0.0000i	-0.5098+0.0000i

Table 3: Transfer function zeros with input V_{ref1} and voltage magnitude outputs (continued)

4.1.3. Phase angle difference input signals

Phase angle differences from bus voltage phasors for buses which are connected to each other are chosen as output signals for this purpose. Tables 4 and 5 show the zeros for the transfer function pairs with input V_{ref1} and bus voltage phase angle differences as outputs, in the approximation of small angle difference, these results would be identical if the output would have been chosen as the active power flow on transmission lines. For the choice of phase angle differences, we get both RHP real zeros as well as RHP complex conjugate pairs.

$\delta_1 - \delta_5$	$\delta_2 - \delta_6$	$\delta_3 - \delta_{11}$	$\delta_4 - \delta_{10}$	$\delta_5 - \delta_6$
-25.0000 + 0.0000i	-25.0000 + 0.0000i	-25.0000 + 0.0000i	-25.0000 + 0.0000i	-25.0000 + 0.0000i
-25.0000 + 0.0000i	-25.0000 + 0.0000i	-25.0000 + 0.0000i	-25.0000 + 0.0000i	-25.0000 + 0.0000i
-0.5000 + 0.0000i	-0.5000 + 0.0000i	-0.5000 + 0.0000i	-0.5000 + 0.0000i	-0.5000 + 0.0000i
-66.6667 + 0.0000i	-66.6667 + 0.0000i	-66.6667 + 0.0000i	-66.6667 + 0.0000i	-66.6667 + 0.0000i
-52.9616 + 0.0000i	-52.9547 + 0.0000i	-52.9574 + 0.0000i	-52.9508 + 0.0000i	-52.9569 + 0.0000i
-52.5897 + 0.0000i	-52.6596 + 0.0000i	-51.4438 + 0.2421i	-52.2005 + 0.0000i	-52.5670 + 0.0000i
-51.8311 + 0.0000i	-51.8310 + 0.0000i	-51.4438 - 0.2421i	-51.3893 + 0.0000i	-51.8307 + 0.0000i

-37.2775 + 0.0000i	-37.2676 + 0.0000i	-38.7965 + 0.2829i	-38.7611 + 0.0000i	-37.2776 + 0.0000i
-13.9756 +10.5595i	-34.5674 + 0.0000i	-38.7965 - 0.2829i	-35.8618 + 0.0000i	-34.8521 + 0.0000i
-13.9756 -10.5595i	-32.9210 + 0.2724i	-13.9095 +10.3511i	-33.8360 + 0.0000i	-13.9526 +10.5348i
-34.4264 + 0.0000i	-32.9210 - 0.2724i	-13.9095 -10.3511i	-32.8666 + 0.0000i	-13.9526 -10.5348i
-33.2840 + 0.0000i	-31.1576 + 0.0000i	-33.5356 + 0.0000i	-31.2231 + 0.0000i	-33.2520 + 0.0000i
-32.7145 + 0.0000i	-28.9086 + 0.0000i	-32.4524 + 0.0000i	-28.7490 + 0.0000i	-32.7470 + 0.0000i
-31.3089 + 0.0000i	-28.7447 + 0.0000i	-31.3458 + 0.0000i	-27.7771 + 0.0000i	-31.2532 + 0.0000i
-28.7492 + 0.0000i	-13.9624 +10.5555i	-28.7484 + 0.0000i	-13.9550 +10.4825i	-28.7493 + 0.0000i
-27.5826 + 0.0000i	-13.9624 -10.5555i	-26.5078 + 0.0000i	-13.9550 -10.4825i	-27.9591 + 0.0000i
-16.4191 + 6.4127i	-22.4648 + 4.4321i	-23.0141 + 5.1229i	-22.9401 + 4.2957i	-16.5488 + 5.4815i
-16.4191 - 6.4127i	-22.4648 - 4.4321i	-23.0141 - 5.1229i	-22.9401 - 4.2957i	-16.5488 - 5.4815i
-22.4597 + 4.4327i	-16.4340 + 4.9603i	-22.7944 + 3.7945i	-20.9298 + 4.2979i	-22.4610 + 4.4325i
-22.4597 - 4.4327i	-16.4340 - 4.9603i	-22.7944 - 3.7945i	-20.9298 - 4.2979i	-22.4610 - 4.4325i
-21.5378 + 0.0000i	-21.4670 + 0.0000i	-21.3465 + 0.0000i	-21.4061 + 0.0000i	-21.4733 + 0.0000i
-20.6480 + 0.0000i	-19.0424 + 0.0000i	5.9128 + 0.0000i	4.6579 + 0.0000i	-19.8660 + 0.0000i
5.8503 + 0.0000i	-0.7860 + 7.4917i	-0.6267 + 8.7550i	-0.8942 + 8.1121i	4.2389 + 0.0000i
-0.7879 + 7.4938i	-0.7860 - 7.4917i	-0.6267 - 8.7550i	-0.8942 - 8.1121i	-0.7880 + 7.4941i
-0.7879 - 7.4938i	-8.7010 + 0.0000i	-0.8361 + 7.9147i	-0.7784 + 6.7899i	-0.7880 - 7.4941i
-0.3190 + 4.9047i	-7.0788 + 0.0000i	-0.8361 - 7.9147i	-0.7784 - 6.7899i	-0.3762 + 4.9746i
-0.3190 - 4.9047i	0.7465 + 4.0467i	-10.1117 + 0.0000i	-11.5941 + 0.0000i	-0.3762 - 4.9746i
-9.1030 + 0.0000i	0.7465 - 4.0467i	-8.4375 + 0.0000i	-8.3848 + 0.0000i	-7.8295 + 0.0000i
-8.6376 + 0.0000i	-3.6327 + 0.0000i	-5.9434 + 0.0000i	-6.1841 + 0.0000i	-8.7642 + 0.0000i
-3.6471 + 0.0000i	-3.2750 + 0.0000i	-3.6376 + 0.0000i	-3.6311 + 0.0000i	-3.6426 + 0.0000i
-3.2864 + 0.0000i	-2.3661 + 0.0000i	-3.2149 + 0.0000i	-3.2254 + 0.0000i	-3.2797 + 0.0000i
-2.4877 + 0.0000i	-1.2885 + 0.0000i	-2.3500 + 0.0000i	-2.3341 + 0.0000i	-2.0727 + 0.0000i
-2.3394 + 0.0000i	-0.7892 + 0.0000i	-1.6984 + 0.0000i	-1.6948 + 0.0000i	-2.4060 + 0.0000i
-0.8610 + 0.0000i	0.1020 + 0.0000i	-0.8707 + 0.0000i	-0.8764 + 0.0000i	-0.8638 + 0.0000i
0.0760 + 0.0000i	-0.4645 + 0.2287i	0.0449 + 0.0000i	0.1229 + 0.0000i	0.0938 + 0.0000i
-0.0709 + 0.0000i	-0.4645 - 0.2287i	-0.0427 + 0.0000i	-0.1100 + 0.0000i	-0.0858 + 0.0000i
-0.5076 + 0.0000i	-0.0994 + 0.0000i	-0.5155 + 0.0000i	-0.5155 + 0.0000i	-0.5083 + 0.0000i
-0.5096 + 0.0000i	-0.5093 + 0.0000i	-0.5099 + 0.0000i	-0.5090 + 0.0000i	-0.5098 + 0.0000i

Table 4: Transfer function zeros with input V_{ref1} and angle difference outputs

$\delta_6 - \delta_7$	$\delta_7 - \delta_8$	$\delta_8 - \delta_9$	$\delta_9 - \delta_{10}$	$\delta_{10} - \delta_{11}$
-25.0000 + 0.0000i	-25.0000 + 0.0000i	-25.0000 + 0.0000i	-25.0000 + 0.0000i	-25.0000 + 0.0000i
-25.0000 + 0.0000i	-25.0000 + 0.0000i	-25.0000 + 0.0000i	-25.0000 + 0.0000i	-25.0000 + 0.0000i
-0.5000 + 0.0000i	-0.5000 + 0.0000i	-0.5000 + 0.0000i	-0.5000 + 0.0000i	-0.5000 + 0.0000i
-66.6667 + 0.0000i	-66.6667 + 0.0000i	-66.6667 + 0.0000i	-66.6667 + 0.0000i	-66.6667 + 0.0000i
-52.9550 + 0.0000i	-52.9567 + 0.0000i	-52.9581 + 0.0000i	-52.9584 + 0.0000i	-52.9613 + 0.0000i
-51.5425 + 0.0000i	-51.4766 + 0.0000i	-51.4052 + 0.0000i	-51.3894 + 0.0000i	-51.4077 + 0.2096i
-51.8536 + 0.0000i	-51.8556 + 0.0000i	-51.8570 + 0.0000i	-51.8573 + 0.0000i	-51.4077 - 0.2096i
-38.7714 + 0.0000i	-38.7541 + 0.0000i	-38.7322 + 0.0000i	-38.7268 + 0.0000i	-38.7912 + 0.3005i

-37.1593 + 0.0000i	-37.1583 + 0.0000i	-37.1572 + 0.0000i	-37.1569 + 0.0000i	-38.7912 - 0.3005i
-33.5680 + 0.0000i	-13.9439 +10.4444i	-13.9644 +10.4748i	-33.6161 + 0.0000i	-13.9502 +10.4255i
-32.5795 + 0.0000i	-13.9439 -10.4444i	-13.9644 -10.4748i	-32.5708 + 0.0000i	-13.9502 -10.4255i
-31.3298 + 0.0000i	-33.5842 + 0.0000i	-33.6091 + 0.0000i	-31.3915 + 0.0000i	-33.5169 + 0.0000i
-28.7487 + 0.0000i	-32.5769 + 0.0000i	-32.5722 + 0.0000i	-28.6025 + 0.0000i	-31.5214 + 0.0000i
-13.9093 +10.4054i	-31.3453 + 0.0000i	-31.3802 + 0.0000i	-28.7523 + 0.0000i	-32.2542 + 0.0000i
-13.9093 -10.4054i	-28.7488 + 0.0000i	-28.7498 + 0.0000i	-13.9674 +10.4806i	-28.7487 + 0.0000i
-25.2402 + 0.0000i	-26.8783 + 0.0000i	-28.3170 + 0.0000i	-13.9674 -10.4806i	-27.7731 + 0.0000i
-22.3846 + 4.4756i	-22.4462 + 4.5212i	-22.6941 + 4.3693i	-22.7443 + 4.3663i	-23.1516 + 4.9680i
-22.3846 - 4.4756i	-22.4462 - 4.5212i	-22.6941 - 4.3693i	-22.7443 - 4.3663i	-23.1516 - 4.9680i
-21.9692 + 4.0608i	-22.4194 + 4.2523i	-22.4514 + 4.4324i	-22.4433 + 4.4327i	-22.8287 + 3.8597i
-21.9692 - 4.0608i	-22.4194 - 4.2523i	-22.4514 - 4.4324i	-22.4433 - 4.4327i	-22.8287 - 3.8597i
-21.3446 + 0.0000i	-21.3881 + 0.0000i	-21.4011 + 0.0000i	-21.4027 + 0.0000i	-21.3829 + 0.0000i
6.8715 + 0.0000i	5.7825 + 0.0000i	4.3950 + 0.0000i	4.0376 + 0.0000i	5.1468 + 0.0000i
-13.1045 + 0.0000i	-0.8958 + 8.2090i	-0.8400 + 8.1860i	-0.8261 + 8.1793i	-0.5673 + 8.6615i
-0.9385 + 8.2224i	-0.8958 - 8.2090i	-0.8400 - 8.1860i	-0.8261 - 8.1793i	-0.5673 - 8.6615i
-0.9385 - 8.2224i	-0.7719 + 7.4484i	-0.7715 + 7.4480i	-0.7714 + 7.4478i	-0.8443 + 7.9069i
-0.7722 + 7.4488i	-0.7719 - 7.4484i	-0.7715 - 7.4480i	-0.7714 - 7.4478i	-0.8443 - 7.9069i
-0.7722 - 7.4488i	-10.4022 + 0.0000i	-8.7953 + 0.1516i	-8.6586 + 0.0000i	-8.6073 + 0.5018i
-8.8441 + 0.0000i	-8.8556 + 0.0000i	-8.7953 - 0.1516i	-8.7057 + 0.0000i	-8.6073 - 0.5018i
-6.7415 + 0.0000i	-6.4174 + 0.0000i	-5.5821 + 0.0000i	-5.2998 + 0.0000i	-5.5367 + 0.0000i
-3.6437 + 0.0000i	-3.6398 + 0.0000i	-3.6315 + 0.0000i	-3.6281 + 0.0000i	-3.6371 + 0.0000i
-3.2587 + 0.0000i	-3.2289 + 0.0000i	-3.1434 + 0.0000i	-3.1020 + 0.0000i	-3.1461 + 0.0000i
-2.4196 + 0.0000i	-2.4200 + 0.0000i	-2.4205 + 0.0000i	-2.4207 + 0.0000i	-2.4430 + 0.0000i
-1.7231 + 0.0000i	-1.7135 + 0.0000i	-1.6879 + 0.0000i	-1.6761 + 0.0000i	-1.6959 + 0.0000i
-0.8660 + 0.0000i	-0.8734 + 0.0000i	-0.8748 + 0.0000i	-0.8761 + 0.0000i	-0.8785 + 0.0000i
0.0001 + 0.0116i	-0.0829 + 0.0000i	0.0684 + 0.0000i	0.0647 + 0.0000i	0.0905 + 0.0000i
0.0001 - 0.0116i	0.0901 + 0.0000i	-0.0640 + 0.0000i	-0.0607 + 0.0000i	-0.0832 + 0.0000i
-0.5155 + 0.0000i	-0.5155 + 0.0000i	-0.5155 + 0.0000i	-0.5155 + 0.0000i	-0.5155 + 0.0000i
-0.5092 + 0.0000i	-0.5092 + 0.0000i	-0.5092 + 0.0000i	-0.5092 + 0.0000i	-0.5097 + 0.0000i

Table 5: System zeros with input V_{ref1} and output angle differences (continued)

It is noticeable that in most of the cases, there are RHP zeros, whereas there is only one path between input and output (there are some closed-loop controls inside each generator) and this is not same as the result we found for the analysis of classic models in [2].

4.2. RHP zero validation by evaluating closed loop poles

As can be seen from the results of previous section, there are some finite RHP zeros in a few cases some of which are close to origin (e.g., the zero at $0.0001 \pm 0.0116i$ for the choice of $\delta_6 - \delta_7$ output in Table 5). We need to examine whether the calculated RHP zeros are truly in the right half plane or they are basically at origin (or even in LHP) and are erroneously computed to be in right half plane due to numerical issues. To do so, a feedback with gain K is implemented between each specified input/output pair. By increasing the gain of feedback, we expect that the poles of the new closed loop system will approach the open loop system (original system) zeros, especially we are looking for finite RHP closed-loop poles. This is performed by manipulating the corresponding entries of the state matrix A. The investigation for different cases are presented below.

For all the following cases, the input is V_{ref} of Generator 1. The closed loop pole calculations are performed for above cases where there are finite RHP zeros. For each case, the eigenvalues of the modified *A* matrix with positive real values are reported. The following cases are considered.

Case I: Output is V_1

For this pair of input/output, there is an open loop RHP zero at +0.0831. The following table shows the change of the desired closed-loop pole with respect to the change in feedback gain.

K	1	1000	10^9
Closed-loop Pole	0.0818	0.0831	0.0831

Table 6: Closed-loop poles with output V_1

It is clear that by increasing the gain *K*, one of closed-loop poles approaches to the open-loop zero. Therefore, the calculated RHP zero for this pair of input and output was truly on RHP and was not due to numerical issues.

Case II: Output is V_6

Similar to previous case, there is an open loop RHP zero at +0.0932. Again, the closed loop poles behave as expected.

K	1	1000	10^9
Closed-loop Pole	0.0832	0.0932	0.0932

Table 7: Closed-loop poles for output V_6

Case III: Output is $\delta_6 - \delta_7$

There are 3 RHP open loop zeros in Table 5. Two of them are very close to the origin.

$$open\ loop\ zeros = \begin{bmatrix} 6.8715 + 0.0000\text{i} \\ 0.0001 + 0.0116\text{i} \\ 0.0001 - 0.0116\text{i} \end{bmatrix}$$

Table 8 shows how three of closed-loop poles evolve by increasing the feedback gain.

K	1	10	1000	10^6	10^9	10^9
Closed-loop Poles	0.0818	0.0958	6.1748 0.0000 + 0.0191i 0.0000 - 0.0191i	6.8706 0.0001 + 0.0116i 0.0001 - 0.0116i	6.8714 0.0001 + 0.0116i 0.0001 + 0.0116i	6.8715 0.0001 + 0.0116i 0.0001 + 0.0116i

Table 8: Closed-loop poles for output $\delta_6 - \delta_7$

This indicates that the complex conjugate RHP zeros were not in the origin and they were indeed correctly calculated in Table 5.

Case IV: Outputs is ω_3

There is an open loop zero equal to +9.1736. This indicates the importance of knowing the presence of RHP zeros. From Table 9, it is clear that the closed loop system is small-signal unstable even for a small gain value of K=1. Clearly this signal is not a good choice for remote control design.

K	1	10	100	1000	10^4	10^6	10^9
Closed-loop Pole	2.8963	6.0272	8.3464	9.0656	9.1624	9.1734	9.1736

Table 9: Closed-loop poles for output ω_3.

In fact, there are also some other closed loop poles at RHP, and they become larger and larger when *K* increases and thus they are not of our interest in this discussion. In fact, they approach to infinite zeros as *K* goes to infinity.

Case V: output is ω_2

Open loop RHP zeros:

$$\begin{bmatrix} 3.9602 + 0.0000i \\ 0.1449 + 3.9105i \\ 0.1449 - 3.9105i \end{bmatrix}$$

Table 10 shows the evolution of the closed-loop poles.

K	1	1000	10^9
Closed-loop Poles	0.1597 + 3.9902i 0.1597 - 3.9902i 2.4270 + 0.0000i	0.1449 + 3.9106i 0.1449 - 3.9106i 3.9574	0.1449 + 3.9105i 0.1449 - 3.9105i 3.9602

Table 10: Closed-loop poles for output ω_2.

4.3. Conclusions on the Zeros Analysis of Detailed Power System Models

We have studied transfer function zeros of specific input-output pairs in detailed power system models of the Kundur test power system. Surprisingly, the studies show the presence of RHP transfer function zeros for many different choices of output signals. The traditional local control design does not have the problem of RHP zeros. In all other cases, the design using remote input signals needs to keep in mind the role played by nonminimum phase zeros and the corresponding complexity of closed loop control performance.

5. Estimation of Zeros from Synchrophasor Data

There are two different approaches in estimating the dynamic modes of power systems: model-based analysis which uses the linearized model of the system around its operating point, and data-based modal analysis which extracts the modal information from the system responses to small or large disturbances. Data-based techniques have some advantages comparing to model-based approaches, such as requiring less computation time and enjoying the real response of the system (i.e., not a response based on system model). Traditionally, there has been little work on estimating the zeros of particular channels in the power grid from measurement data. In this section, we will discuss data-based techniques for estimating zeros, focusing on Right Half Plane (RHP) zeros.

5.1. Available Techniques

The techniques for identifying RHP zeros can be categorized into two main groups. First, approaches that only determine the existence of RHP zeros, and second, approaches that estimate the values of zeros so that from the numerical results, we can identify the RHP zeros.
For the purpose of only identifying the existence of RHP zeros (not evaluating their values), let us examine the application of two traditional methods:

5.1.1. Observing undershoot in the step response of the system

It is known that for a system with RHP zeros, undershoot is expected in the step response of the system, vice versa. However, this is true only when the initial conditions of the system states are zero. The following counterexample shows how specific initial conditions may produce undershoot in the step response of a minimum-phase system. Let us consider a system with the following matrices:

$$A=\begin{bmatrix}-1 & -30\\ 1 & -1\end{bmatrix}, B=\begin{bmatrix}-1\\ 1\end{bmatrix}, C=\begin{bmatrix}1 & 0\end{bmatrix}, D=0$$

The transfer function of the system is:

$$T=\frac{s+31}{s^2+2s+31}$$

Also let us consider the initial condition as $x_0=\begin{bmatrix}4\\ -1\end{bmatrix}$.
The response of the system to the input of step is shown in Figure 6 below.

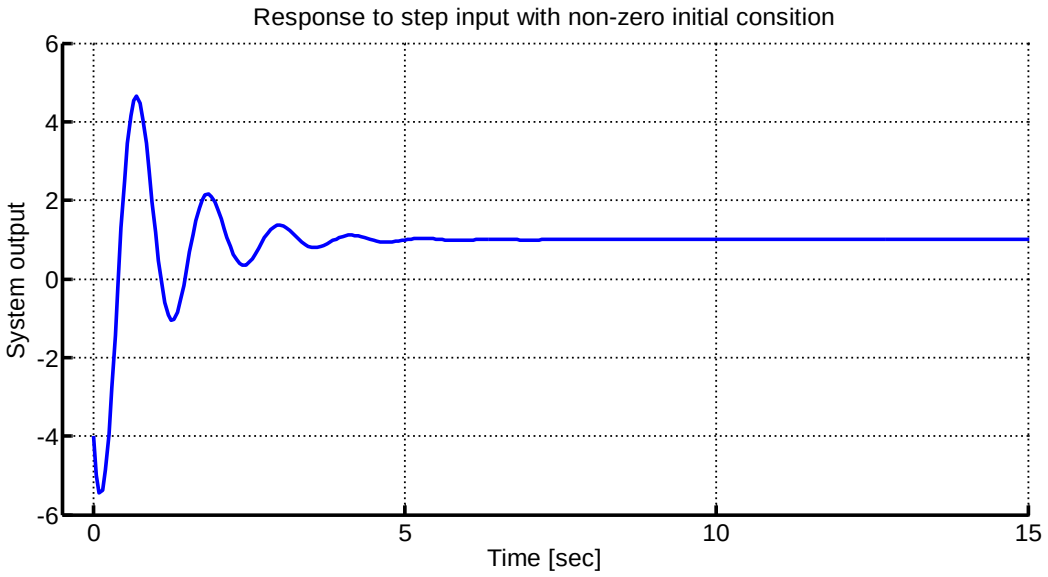

Figure 6: Response of a minimum-phase system to the input of step function

Moreover, the response of the system to the same input with initial condition $x_0 = \begin{bmatrix} 1 \\ 0 \end{bmatrix}$ is depicted in Figure 7.

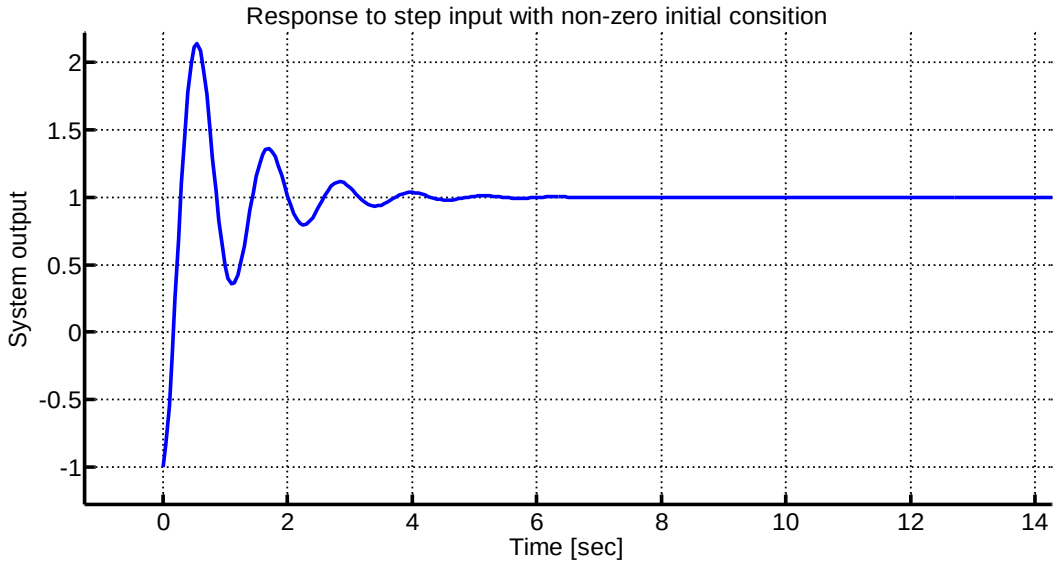

Figure 7: Response of a minimum-phase system to the input of step function.

Comparing the two responses, based on observing undershoot in the response of system, the existence of RHP zero cannot be concluded.

In the case of power systems, even if we assume that the applied disturbance is a step function, we cannot justify the existence of RHP zeros from the response with undershoot, since the power

system had been operating (ambient condition) before the appliance of disturbance and the initial conditions had not been zero. Moreover, because of non-linear behavior of power systems, especially at the beginning of oscillations, even with other conditions satisfied, we cannot justify the existence of RHP zero based on undershoot, since it could be true only for linear systems.

5.1.2. Identifying non-minimum phase behavior from the Fourier phase plot

It is known that for both of minimum-phase and non-minimum phase systems, after frequencies of transfer function zeros, there is a 20dB/dec increase in the magnitude of Bode plot of the transfer function of the systems. Thus, at each frequency that the magnitude is increased we can expect a zero. For minimum-phase systems, there will be a 90 degree increase in the phase plot around that zero frequency, however, for non-minimum phase systems, there will be a 90 degree decrease in the phase plot. Therefore, depending on the increase or decrease in the phase plot (after detecting an increase in the magnitude plot), we can identify whether the zero is in RHP or LHP.
Since we aimed to identify the RHP zeros from the system measurements and we do not have the bode plot of transfer function, we can use the magnitude and phase plots of the Fourier transform of the output (which includes both of input and transfer function poles and zeros). In fact, considering the period of the applied brake very short, we can consider it as impulse function.
In the figure 8, the response of a real power system to a brake test is shown.

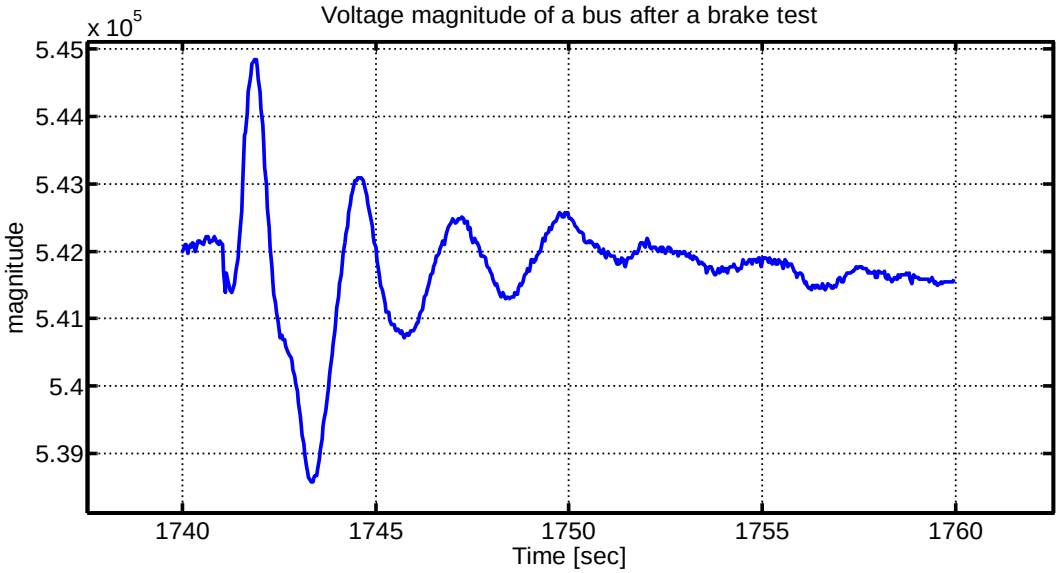

Figure 8: Voltage magnitude of a bus at WECC system after a brake test.

The non-linear part (the first three seconds) as well as the ambient part (the last five seconds) are removed for the purpose of FFT analysis. The magnitude and the phase plots of FFT (of the linear part) of the signal in the frequency range of 0.1HZ to 2Hz are shown below in Figure 9.

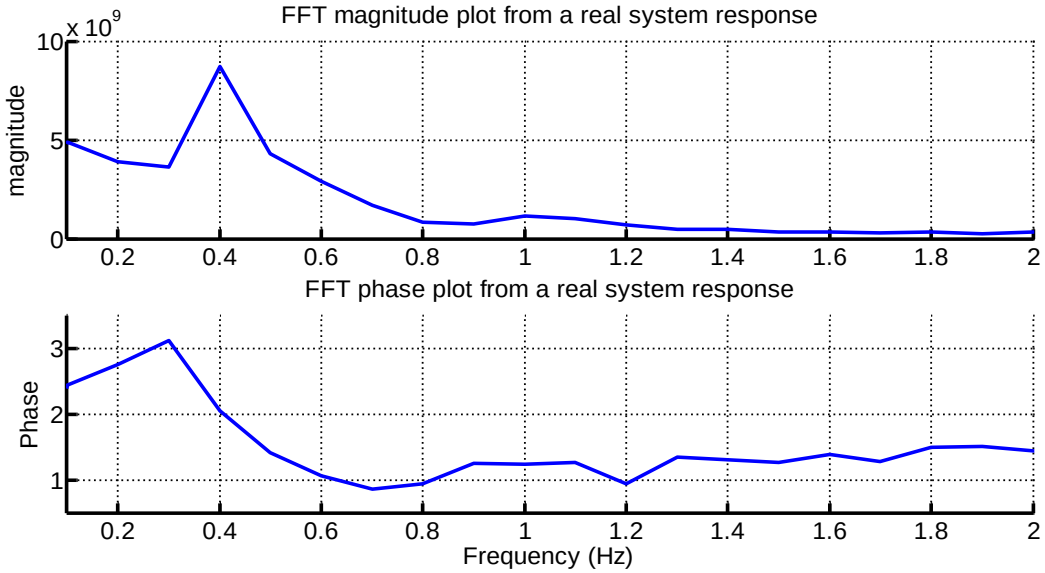

Figure 9: FFT magnitude and phase plots of the WECC brake test signal.

The described pole and zero property cannot be seen in the above figures, since it seems that the input is not an ideal impulse and its frequency content is mixed into that of output. Another issue with this type of identification is that the brake cannot be considered as an input, in fact, even if we can model the brake as an input, it is not of our interest in the sense of system control.

5.1.3. Subspace techniques for numerically evaluating zeros

As observed in two previous sections, traditional methods were not able to determine the existence of RHP zeros. In this section, the application of subspace techniques in numerically evaluating zeros will be investigated. In general, subspace methods estimate the set of A, B, C, and D matrices for a system whose input and output are given. It is noticeable that the estimated matrices are not unique in general, since for state space representation of a system, infinitely many states sets can be considered.

One of the most powerful subspace techniques is N4SID (Numerical algorithms for Subspace State Space System IDentification) method [26]. The method is already applied to power system probing data to estimate the system electromechanical modes [27]. However, its performance is not evaluated for estimating the zeros. In one of the steps of the method, a weighted SVD calculation should be performed. Depending on different weighting matrices used in the SVD process, different subspace methods are introduced such as Canonical Variate Algorithm (CVA) [28] and Multivariable Output Error State sPace (MOESP) [29].

The biggest challenge in using the subspace methods is determining a suitable model order that usually requires a trial and error procedure. Moreover, Akaike's Information theoretic Criterion (AIC) [30] can be used for determining the suitable model order.

In what follows, the application of N4SID on estimating the poles and zeros of a synthetic fifth-order system is investigated. The system is excited with a white Gaussian noise plus a DC value. The transfer function of the system is shown below.

$$H(s) = \frac{(s^2 + 3s + 8)(s^2 - 0.5s + 4)}{(s^2 + s + 1)(s^2 + 2s + 3)(s + 4)}$$

where there are a pair of RHP complex conjugate zeros and a pair of LHP complex conjugate zeros. A canonical model realization is considered and then arbitrary initial condition is chosen. To get more reliable results, a Monte-Carlo simulation with 50 independent inputs is performed. Each input is analyzed with 58 sixty-sec moving windows. The Matlab routine *n4sid* is used for implementing the method.

The output of system related to one of the 50 simulations is shown below. The transient portion of the signal is not shown here.

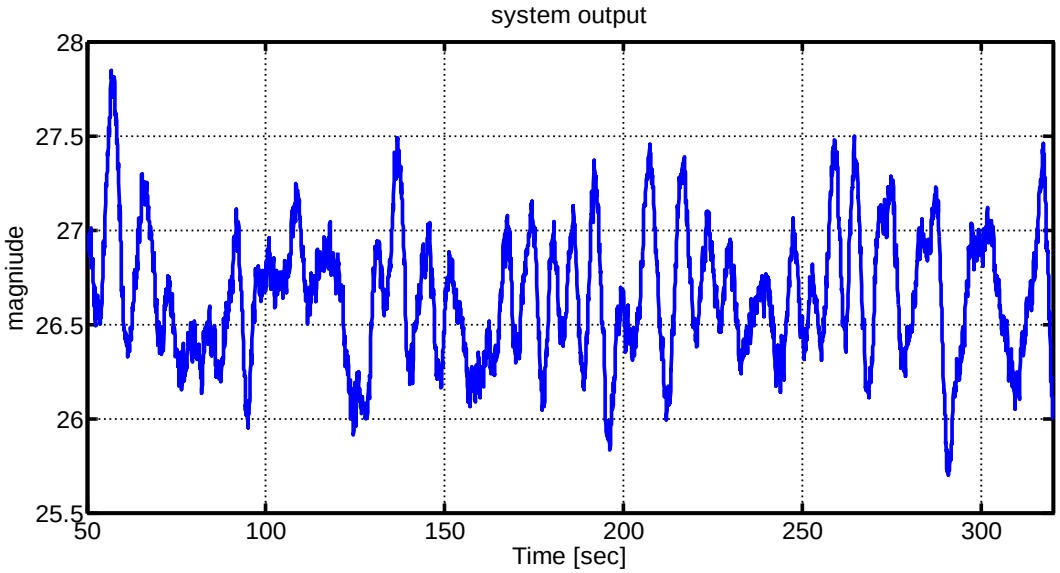

Figure 10: Random input to the fifth-order synthetic system.

After estimating the system matrices at each window, five poles as well as four finite zeros are calculated based on the eigenvalues of the A matrix and generalized eigenvalues of $\begin{bmatrix} A & B \\ C & D \end{bmatrix}$, and $\begin{bmatrix} I & 0 \\ 0 & 0 \end{bmatrix}$ matrices, respectively. The poles estimates are shown in figure 11. The true value is shown with a red circle.

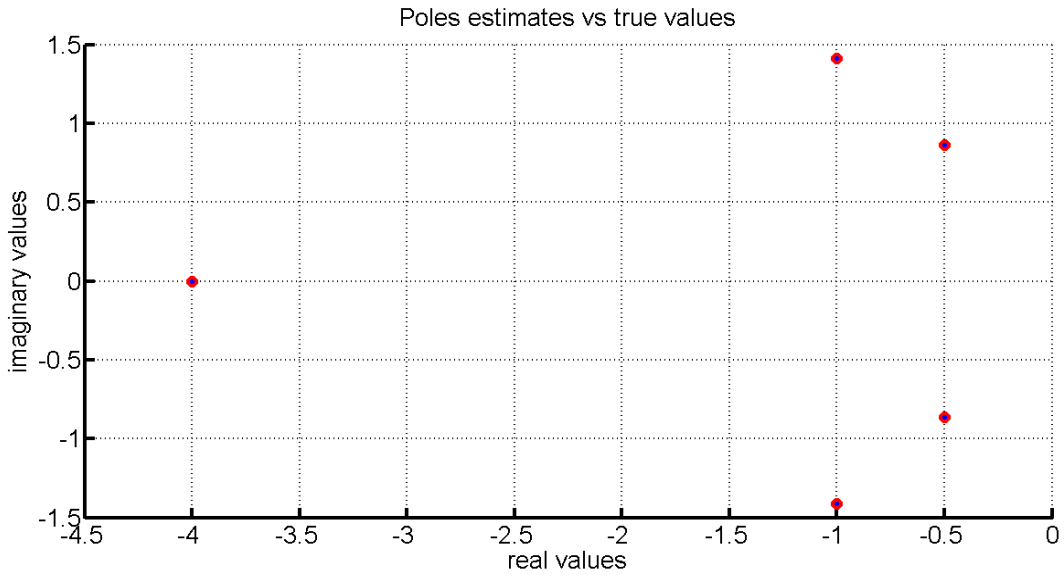

Figure 11: Poles estimates of the fifth-order synthetic system.

As can be seen, the poles of the system are exactly estimated in all windows. Now, let us examine the accuracy of zero estimation. The zero estimates are shown in Figure 12.

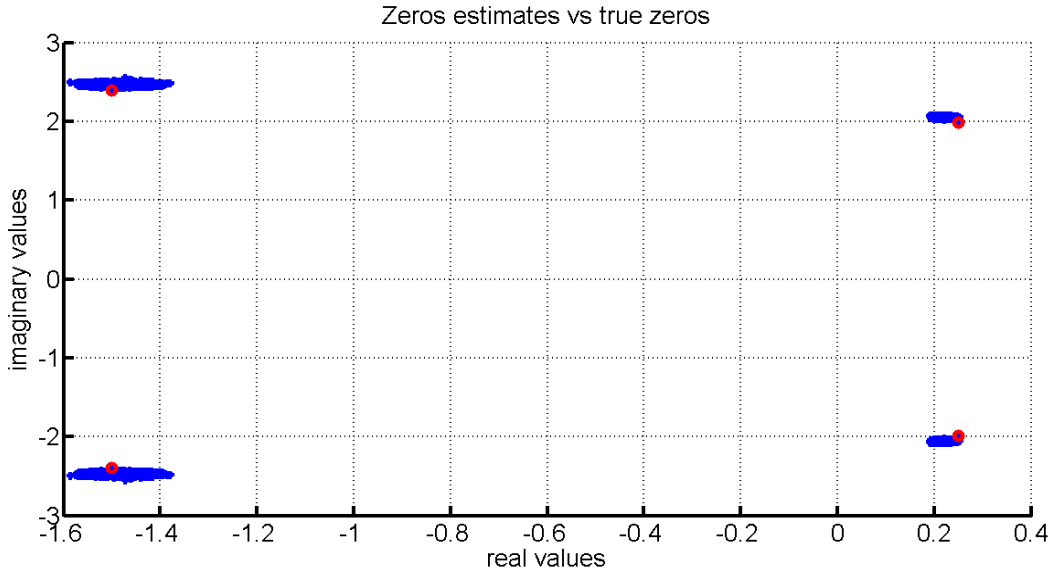

Figure 12: Zero estimates of the fifth-order synthetic system.

Both of the RHP and LHP zeros are identified with small bias and variance.

The results obtained by N4SID are not always as good as shown above. In fact, by performing many simulations, it is observed that we may obtain estimates with small bias and small variance

(like above estimates), small variance but not small bias, and estimates with not negligible bias and variance. We are still looking for the reason of occurrence of the second and third types. To provide an example of the third case, let us consider the following system.

$$H(s)=\frac{(s+3)(s^2-s+3)(s^2+5s+18)(s^2+9s+25)(s^2-4s+7)}{(s^2+0.5s+1)(s^2+6s+12)(s^2+8s+18)(s^2+14s+50)(s+6)(s+8)}$$

The same procedure as previous system is made for this system. The model order 10 is chosen and a Monte Carlo simulation is performed. The poles and zeros estimates are shown in figures 13 and 14.

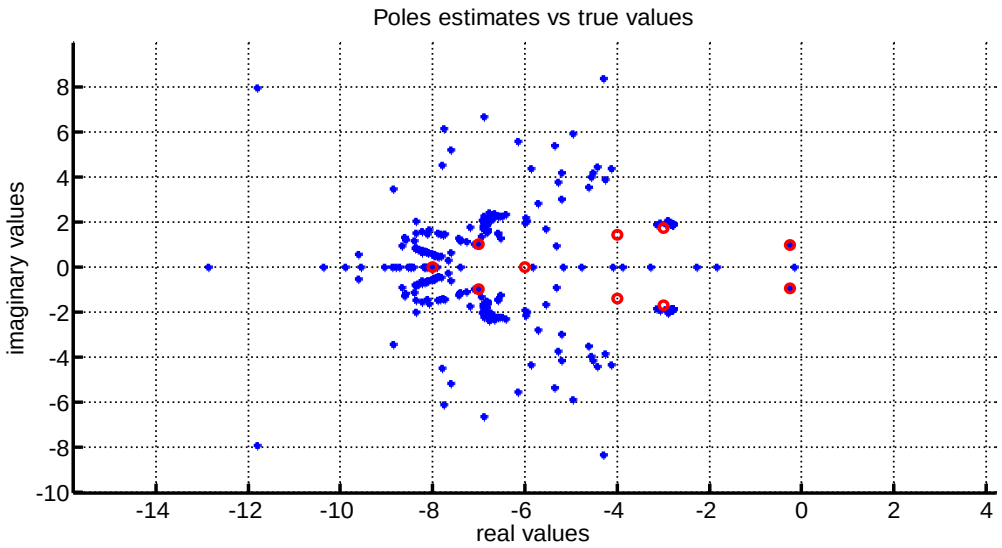

Figure 13: Poles estimates of the tenth-order synthetic system.

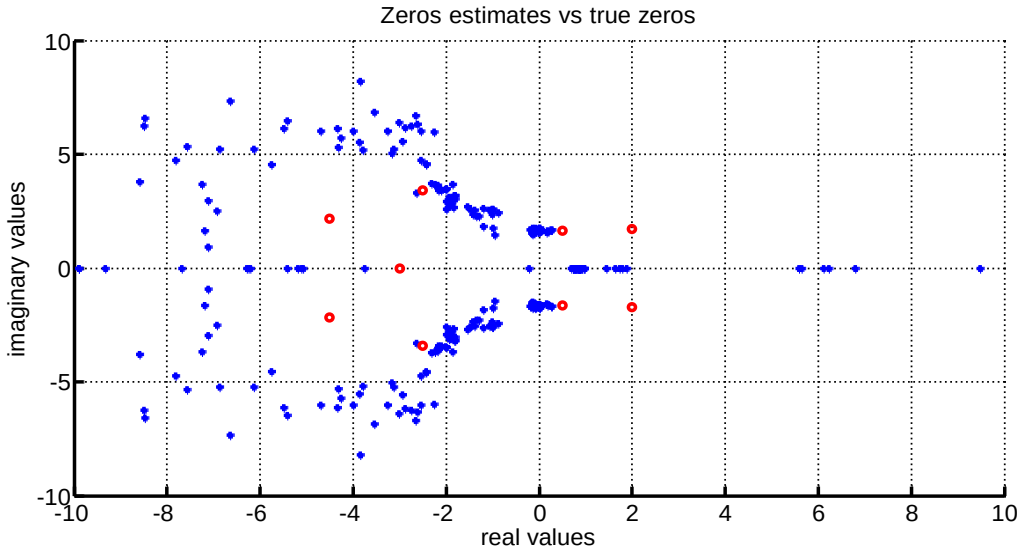

Figure 14: Zeros estimates of the tenth-order synthetic system.

None of pole or zero estimates are satisfactory. One reason for getting inaccurate results is that the second system has higher order and is more complex. The model order 10 is not so large and as we will see, choosing model orders as large as 10 is usual for power systems. The two cases we studied, we used a single input and single output for identification. Now, let us examine the multi-channel analysis for the zero estimation problem.

Single input multiple output N4SID technique

In employing the N4SID for estimating the poles of the system using probing data, authors of [27] have considered power system as a SIMO system where single input but multiple outputs are used. This is because of the fact that poles are common in all outputs of the system. However, the zeros between each pair of input and output are different. Therefore, we need to be careful. In the application of N4SID in a SIMO case, a common *A* matrix is estimated for the whole system. Moreover, since only one input is considered for the system, the dimension of *B* will be same as the SISO case. However, the dimension of *C* matrix depend on the number of employed outputs. In other words, if *m* outputs are employed, there will be *m* rows in the *C* matrix and each row corresponds to one output. Thus, for estimating the zeros between the input and a specific output, we should use the A and B matrices along with the corresponding row of the *C* matrix. Now, let us examine the previous 10^{th} order system in two cases. In the first case, the single input with five outputs are analyzed whereas in the second case, ten outputs are employed.

Case I: A multi-channel analysis with five outputs

The poles and zeros estimate are shown in the figures 15 and 16.

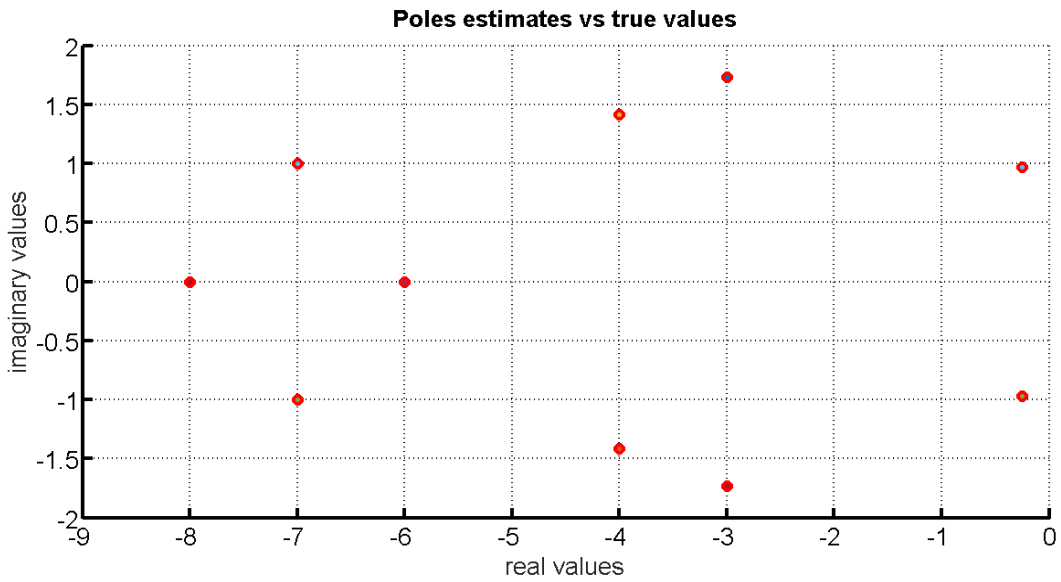

Figure 15: Multi-channel pole estimates of the tenth order system with five outputs.

Comparing to Figure 13, the pole estimates have significantly improved and all estimates (in all windows of all Monte Carlo iterations) match with true values (all estimates are inside the red circles (true values)).

The zero estimates are depicted in figure 16. Comparing to figure 14, the zero estimates have also significantly improved. Most of the estimates are inside the red circles (true values). However, there are some biased estimates for the zero at $-2.5000 \pm 3.4278i$. Moreover, there are some estimates between real values 0 and -2 which do not correspond to any of true zero values. Besides, some spurious zeros in the right hand side of the real axis are estimated which again do not correspond to any of zeros.

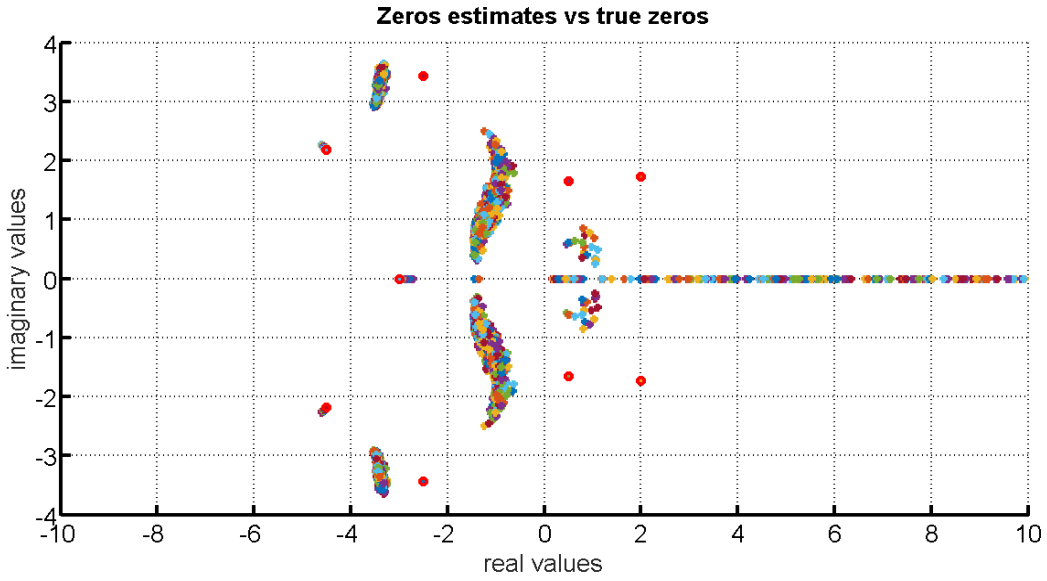

Figure 16: Multi-channel zero estimates of the tenth order system with five outputs

Case II: A multi-channel analysis with ten outputs

In this case, the single input along with 10 outputs in a same Monte Carlo simulation are employed and the estimates are shown in figures 17 and 18.

As can be seen in figure 17, the pole estimates are perfect which is expected since even with five outputs, they were estimated accurately.

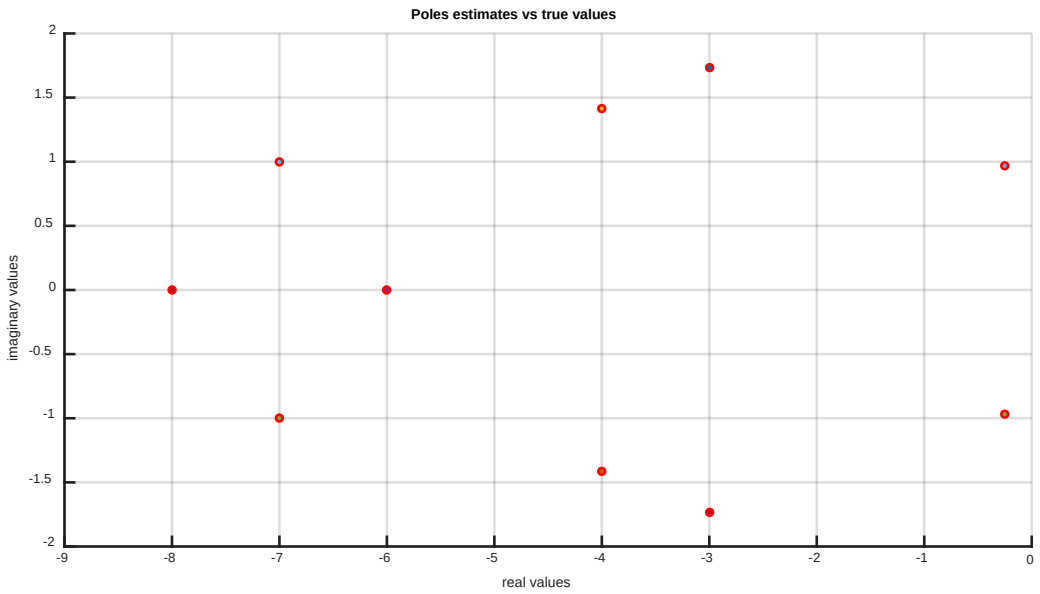

Figure 17: Multi-channel pole estimates of the tenth order system with ten outputs.

The results for zero estimation are demonstrated in figure 18. Comparing to figure 16, there are no spurious zeros on the right hand side of the real axis any more. Moreover, the biased estimates between real values -2 and -4 are now closer to their true value (i.e., they are less biased). The number of zeros with real values between -2 and -4 are less and also closer to the true zero at -3. Considering the mentioned fact, by increasing the number of employed outputs from five to ten, the zero estimates have significantly improved.

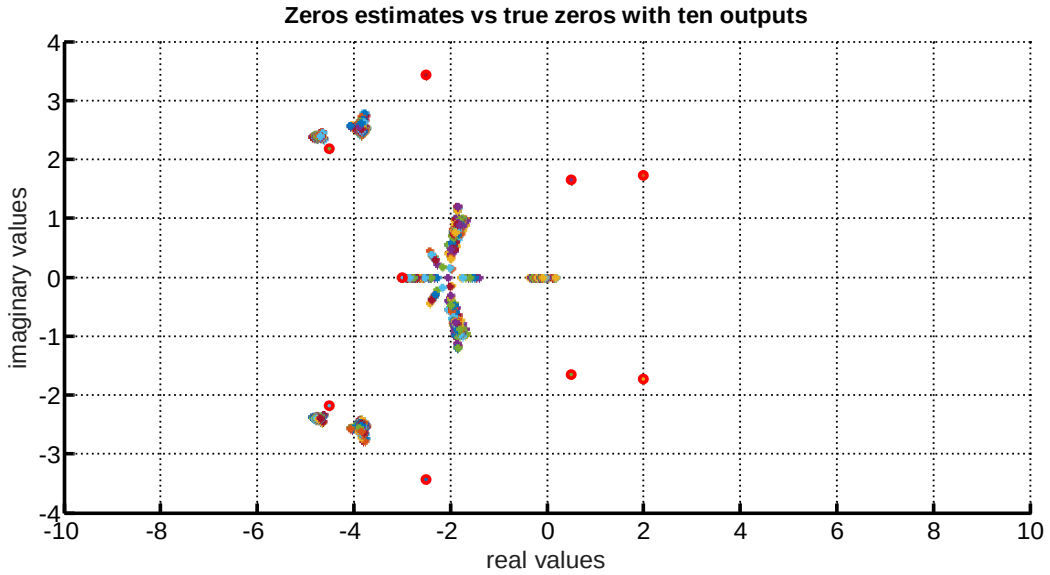

Figure 18: Multi-channel zero estimates of the tenth order system with ten outputs.

5.1.4. Discussion

- Comparing cases I and II, it is obvious that employing more outputs, we can improve the accuracy of estimates
- As can be seen in all previous cases, the accuracy of zeros estimation is not as good as that of poles estimation. Thus, we tried the idea of inverse system as well as improving the N4SID accuracy using Prediction Error Minimization (PEM) approach as follows.

5.1.5. Inverse system idea

From the results of N4SID technique, it can be understood that the accuracy of N4SID in estimating the poles of a transfer function is better than its accuracy in estimating zeros. In order to solve the problem, we tried the idea of [31] in building an imaginary inverse system for the system to be analyzed where the transfer function of the inverse system is the inverse of the transfer function of the original system. Therefore, by finding the poles of the inverse system we find the zeros of the original system which are of our interest.

Theorem

Let $H(s)=C^T(sE-A)^{-1}B+D$ be the transfer function of the descriptor $\Sigma=(E,A,B,C,D)$, and let $H_z(s)=C_z{}^T(sE_z-A_z)^{-1}B_z+D_z$ be the transfer function of the augmented descriptor realization $\Sigma_z=(E_z,A_z,B_z,C_z,D_z)$ where

$$A_z=\begin{bmatrix}A & B\\ C^T & D\end{bmatrix}, E_z=\begin{bmatrix}E & 0\\ 0 & 0\end{bmatrix}, B_z=\begin{bmatrix}0\\ -I_m\end{bmatrix}, C_z=\begin{bmatrix}0\\ I_m\end{bmatrix}, D_z=0$$

and I_m is the $m\times m$ identity matrix. Then $H_z(s)=H^{-1}(s)$.

In order to calculate the poles of the inverse system Σ_z (which are the zeros of the original system), equation $\det(sE_z-A_z)=0$ should be solved. In other words, values of *s* that drops the rank of the following matrix $\begin{bmatrix}A-sE & B\\ C^T & D\end{bmatrix}$ below its normal rank should be found. This is the same result as we found earlier for calculating the zeros of a system by solving the generalized eigenvalue problem $eig(\begin{bmatrix}A & B\\ C^T & D\end{bmatrix},\begin{bmatrix}E & 0\\ 0 & 0\end{bmatrix})$.This method originally is proposed to calculate the dominant zeros of a system based on calculation of dominant poles of an (inverse) system by means of some methods like Arnoldi approach. In fact, it does not improve the estimation of original system matrices and as much as matrix A is accurately estimated, but matrices B and C are poorly estimated in N4SID method, calculating zeros by calculating the poles of the inverse system will not be effective. In fact, we should improve the accuracy of B and C matrices to get more accurate zeros. However, when we have accurate enough B and C matrices, using the idea of inverse system

would be computationally effective. Simulations verify the above discussion, but are not provided here for the sake of brevity.

5.1.6. Application of Prediction Error Minimization technique for improving the N4SID estimates

Prediction Error Minimization (PEM) technique is developed to improve the estimation of the parameters of a model which are previously identified by another technique such as N4SID method. The basic idea is to express the predicted value of output at time N (i.e., $\hat{y}(N)$) in terms of model parameters as well as past input and output samples and then minimize the distance between the measured output values and the predicted values, i.e., finding $\hat{\theta}_N = \arg\min_{\theta} V_N(\theta)$ where $V_N(\theta) = \sum_{t=1}^{N} l(y(t) - f(Z^{t-1}, \theta))$ and $Z^N = \{u(1),y(1),u(2),y(2),...,u(N),y(N)\}$ is the collection of past data up to time N , θ is the set of system parameters to be estimated and *l* is a suitable distance measure such as the second norm [32].
For employing PEM, first, an initial model of system is estimated by N4SID and then improved by PEM technique. Although, the whole process is more time consuming, the results are slightly more accurate.

5.2. General observations about simulations and improvements

5.2.1. Effect of analyzing window length on the accuracy of estimates

Windows with different length from 60 seconds to 300 seconds are used to estimate the zeros of different systems. The results show that increasing the window length more than 60 seconds does not have a noticeable effect on the variance and bias of estimates, whereas it significantly increases the computation time, thus, based on experiments, a window of length 60 sec would be accurate enough.

5.2.2. Effect of sampling frequency on the accuracy of estimates

In order to investigate the effect of sampling frequency on the accuracy of estimates, sampling frequencies 20, 30, and 40 Hz are used for a couple of systems. The results show that using higher sampling rates slightly improves the bias and variance of estimates, however, employing higher sampling frequencies requires more computation time, thus the sampling frequency 20Hz is used in simulations.

5.2.3. Filtering the data

In order to remove the undesirable component of a signal, preprocessing is usually performed using filters before analyzing a signal. By filtering the data, the transfer function of the filter will be multiplied to the Laplace (Z) transform of the output. Thus, filtering the output will not affect the zeros estimation. However, removing the DC part of the output falsify the estimates. Let us consider $U(s)$, and $Y(s)$ as the Laplace transform of input and output of a system, respectively. If we remove the DC part of $y(t)$ and call it $\hat{y}(t)$, then the new transfer function (i.e., between $\hat{y}(t)$ and $u(t)$) would be:

$$\hat{H}(s)=\frac{\hat{Y}(s)}{U(s)}=\frac{Y(s)-\frac{1}{s}y_{DC}}{U(S)}=\frac{Y(s)}{U(s)}-\frac{1}{s}\frac{y_{DC}}{U(s)}=H(s)-\frac{1}{s}\frac{y_{DC}}{U(s)}\xrightarrow{\text{assuming } U(s)=\frac{1}{s}}H(s)-y_{DC}$$

$$if\ \text{H(S)}=\frac{N(s)}{D(s)}\rightarrow\hat{H}(s)=\frac{N(s)-(y_{DC})(D(s))}{D(s)}$$

It can be concluded that while removing the DC part does not change the poles of the estimation, it significantly changes the estimated zeros.

Example: Let's consider the previous second-order system with the following transfer function:

$$T=\frac{1.01s-0.398}{s^2+0.5s+8.06}$$

The response of the system to step function is used. The estimates are shown in figure 19.

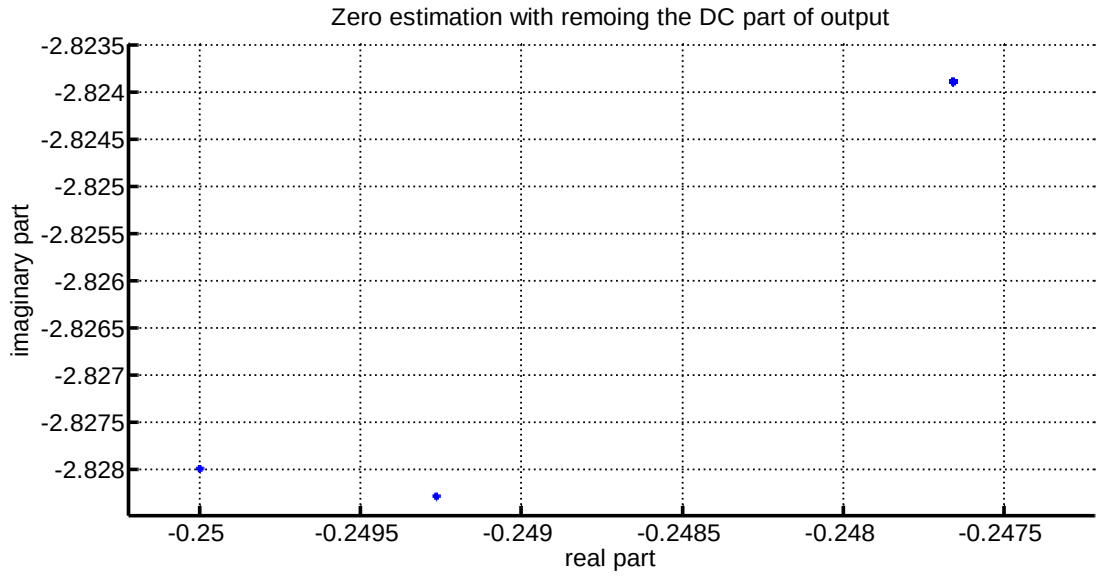

Figure 19: zero estimate with filtering output

(It should be noted that so most of the estimated zeros are at $s=-0.2477-2.8239i$, thus shown as a single point. Besides, the complex conjugate part is not shown.)

Instead of a single RHP zero, two LHP complex conjugate zeros are estimated. Based on the results, it is verified that removing the output offset significantly affects the zero estimation, thus caution should be exercised in preprocessing procedure.

5.3. Non-minimum Phase Characteristics in Simulated Power System Response

In this section, the zeros dynamics of the well-know 2-area Kundur system will be investigated. System description: The single line diagram of the system is shown below. Each generator is equipped with exciter, governor, and PSS and modeled with nine states. The Generator 1 is considered as slack generator. Moreover, the loads are modeled as 50% constant power and 50% constant impedance.

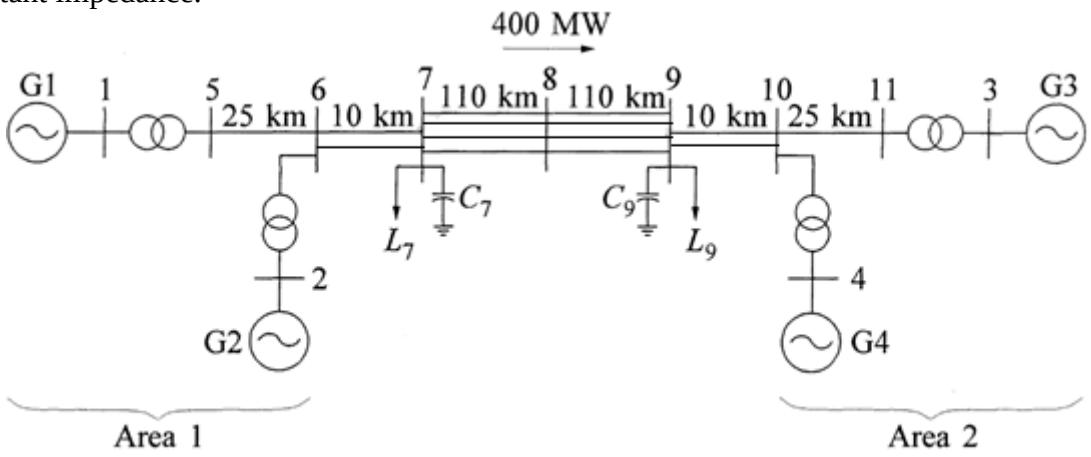

Figure 20: Two-area Kundur test system.

The structure of study will be as follows. First, small-signal analysis of the system will be performed to obtain the true values of poles and zeros based on the model. Second, In order to demonstrate the consistency of the provided transient simulator with small signal simulator, a data-based modal analysis technique is applied to the system response to a large disturbance and the obtained modes are compared with those of small signal analysis. In the third step, probing signal is injected into the system and system responses are obtained. By both of input and output in hand, N4SID technique will be employed to get the zeros of desirable input and output pairs.

5.3.1. Small signal analysis

For performing the small signal analysis of the system, a code is written in MATLAB (mfile). Since it is not related to our discussion, participation factors, mode shapes, etc. are not presented here and only poles and zeros are demonstrated. Dominant poles and zeros are highlighted in green.

Eigenvalues	Modes frequency (Hz)	Mode damping factors (%)
-93.3070 + 0.0000i	0	100.0000
-90.4807 + 0.0000i	0	100.0000
-74.8378 + 0.0000i	0	100.0000

-43.7733 + 0.0000i	0	100.0000
-47.0286 + 0.0000i	0	100.0000
-46.8879 + 0.0000i	0	100.0000
-29.5279 + 0.0000i	0	100.0000
-2.1262 + 8.5125i	1.3548	24.2329
-2.1262 - 8.5125i	1.3548	24.2329
-1.8617 + 6.9984i	1.1138	25.7079
-1.8617 - 6.9984i	1.1138	25.7079
-10.8303 + 0.0000i	0	100.0000
-8.8399 + 0.0000i	0	100.0000
-0.6059 + 3.2405i	0.5157	18.3790
-0.6059 - 3.2405i	0.5157	18.3790
-4.8539 + 0.0000i	0	100.0000
-3.9656 + 0.0000i	0	100.0000
-3.2216 + 0.0000i	0	100.0000
-0.1778 + 0.0000i	0	100.0000
-0.1794 + 0.0000i	0	100.0000
-0.1798 + 0.0000i	0	100.0000
-0.1031 + 0.0000i	0	100.0000
-0.1021 + 0.0000i	0	100.0000
-0.1009 + 0.0000i	0	100.0000
-0.1000 + 0.0000i	0	100.0000
-0.1000 + 0.0000i	0	100.0000
-0.1000 + 0.0000i	0	100.0000

Table 11: Eigenvalues of Kundur test system obtained from small signal analysis.

In the next step, the voltage reference of Generator 2 is considered as input and the speed of generator 2 is considered as output. The calculated zeros for this pair of input and output is presented in the following table.

No.	Zeros
1	Inf + 0.0000i
2	Inf + 0.0000i
3	-0.1852 + 0.0000i
4	-50.0000 + 0.0000i
5	-0.1000 + 0.0000i
6	-93.1160 + 0.0000i
7	-76.5595 + 0.0000i
8	-46.8896 + 0.0000i
9	-44.6984 + 0.0000i
10	-26.8286 + 0.0000i
11	-2.1299 + 8.4182i
12	-2.1299 - 8.4182i
13	-8.9346 + 0.0000i

14	-0.6856 + 3.3797i
15	-0.6856 - 3.3797i
16	-3.2605 + 0.0000i
17	-5.4532 + 0.0000i
18	-4.9270 + 0.0000i
19	-0.1030 + 0.0000i
20	-0.1010 + 0.0000i
21	-0.1776 + 0.0000i
22	-0.1799 + 0.0000i
23	Inf + 0.0000i
24	-0.1000 + 0.0000i
25	-0.1000 + 0.0000i
26	0.0000 + 0.0000i
27	-0.1000 + 0.0000i
28	Inf + 0.0000i

Table 12: Zeros of Kundur test system obtained from small signal analysis.

As can be seen from the above table, there is no RHP zero for this input and output.

5.3.2. Transient analysis

A transient simulator is prepared in Matlab (mfile) to get the system responses to our inputs of interest. Before getting the system response to desirable inputs (i.e., probing signal), the validity of the provided code and its consistency with the small signal code is investigated by finding and comparing the system modes which are found by applying multi-dimensional Prony analysis to system responses to a large disturbance. For producing a large disturbance, a fault in the middle of one of four lines between buses 8 and 9 is applied for 6 cycles and then the fault is cleared and the line is reclosed and the transient response of system on all 27 dynamic states and 21 network states are obtained. The multi-channel Prony analysis is applied to channels with highest observability of modes of interest and the estimated poles are compared to the ones obtained by small signal analysis.

Among all obtained signals, $\theta_2, \omega_2, \theta_3, \omega_3, \theta_4, and\ \omega_4$ have the highest observability for the inter-area mode (i.e., the mode with frequency 0.5157Hz). They are given to the multi-channel Prony analysis and the results are shown in the following table (spurious modes are not shown).

NO.	Mode frequency	Mode damping
1	0.5173	17.5802
2	1.0345	17.5819
3	1.1245	23.9334

Table 13: Modal analysis results from Prony analysis.

The results are consistent with those of small signal analysis, especially for the inter-area mode which is the dominant mode in all signals.

5.3.3. Probing analysis

Different probing signals whose level, frequency content, and duration are under control have been designed and tested on the WECC system such as brake insertion, single-mode square wave (SMSW), and Low-Level Pseudo-Random Noise (LLPRN) [27]. Figure 21 shows the MW line flows response of LLPRN and SMSW tests by HVDC modulation at the Celilo terminal of the Pacific HVDC Intertie (PDCI) on the Celilo #3 line which is one of four ac system feeds into the PDCI at Celilo.

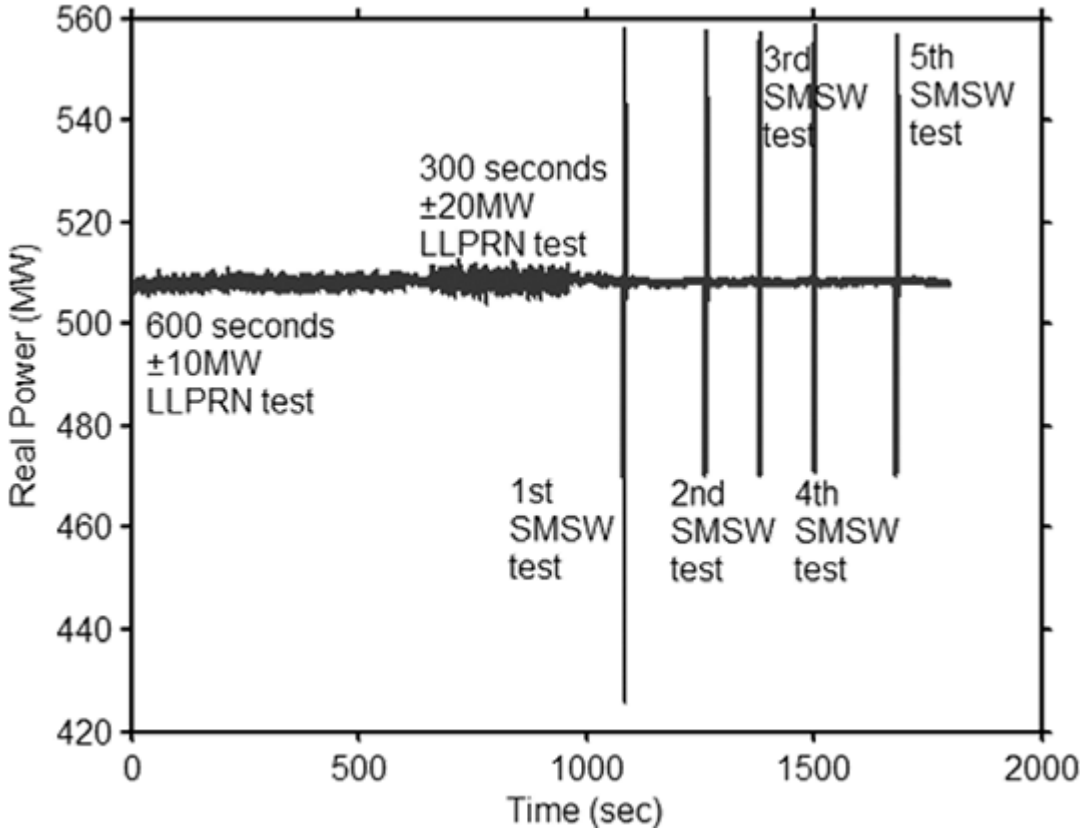

Figure 21: probing test response in WECC system [33].

In order to perform the probing test on Kundur system, the voltage reference of Generator 2 is modulated with Gaussian white noise which is filtered using a bandpass filter between frequencies 0.05Hz and 0.9 Hz [2] while other generators voltage references are kept constant.
Taking the system responses along with the measureable injected input into the system, we will examine the input/output characteristics of pairs of interest. First let us examine the estimated poles using the same signals used in Prony analysis (i.e., $\theta_2, \omega_2, \theta_3, \omega_3, \theta_4, and\ \omega_4$) along with the input. The model order 10 is chosen for this purpose. A Monte-Carlo simulation with 50

independent inputs is performed. Figures 22 and 23 show the electromechanical modes estimation. As can be seen the dominant inter-area mode (with frequency 0.5157Hz and damping ratio 18.37%) is estimated with a very small bias and variance. Moreover, two other electromechanical modes, although close to each other, are distinguished with good biases and acceptable variances.

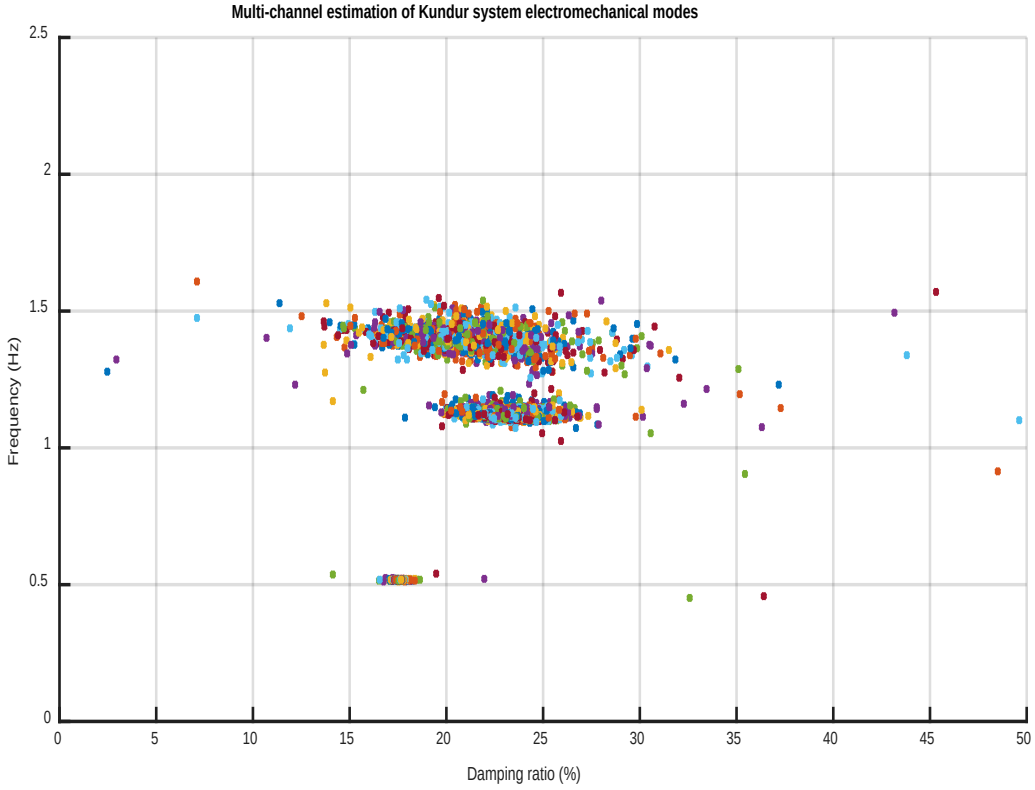

Figure 22: Frequency-damping plot of Kundur system modes by multi-channel N4SID technique.

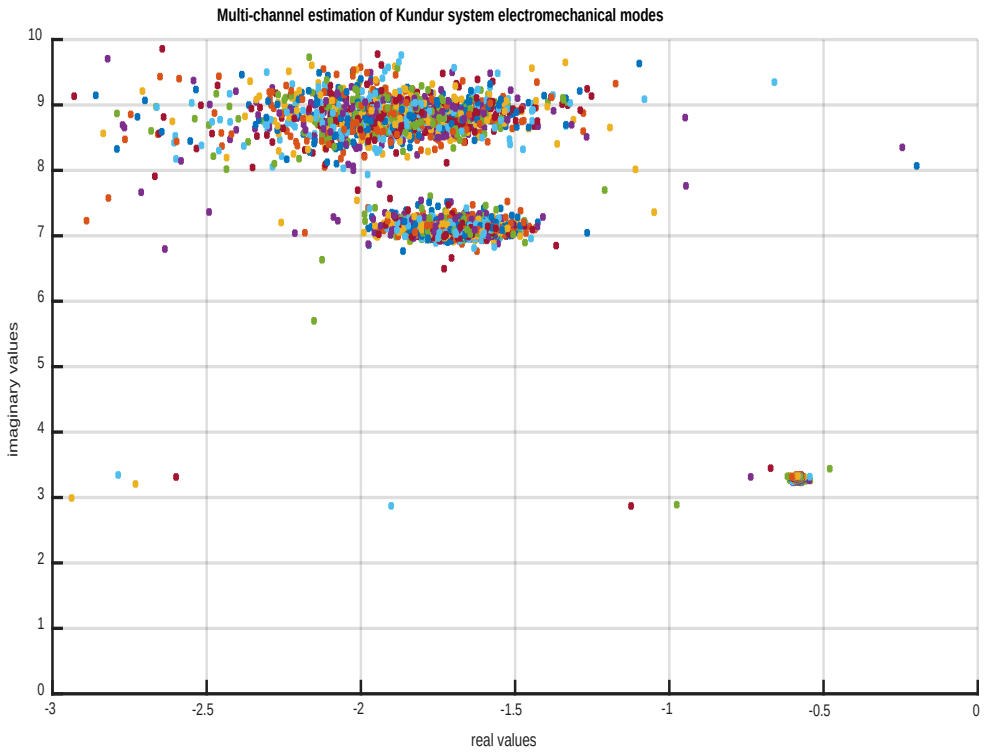

Figure 23: Real-Imaginary part plot of Kundur system modes by multi-channel N4SID technique.

Comparing to the small signal analysis results, the accuracy of poles estimate is satisfactory. There are also some spurious (based on their frequencies) modes which are discarded.

SISO analysis for zero estimation

Now let us employ the speed of Generator 2 as output (along with input) with model order of 10. The estimated zeros are presented in the figure 24.

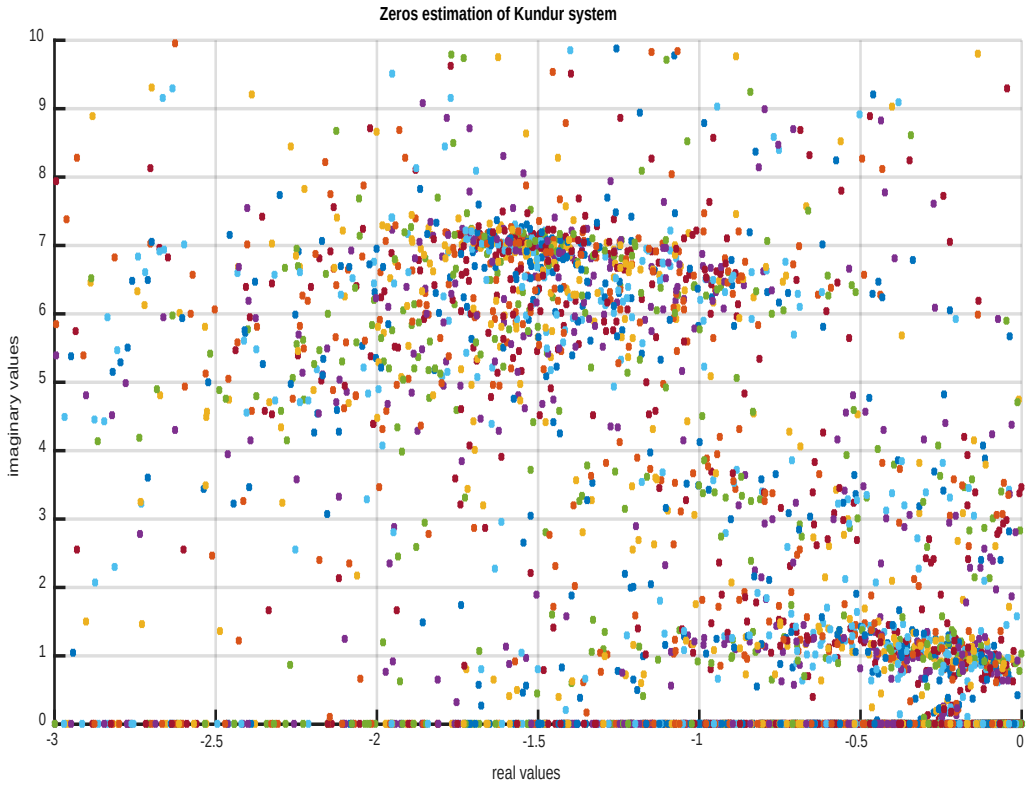

Figure 24: Real-Imaginary part plot of Kundur system zeros by N4SID technique.

As can be seen, the dominant zeros which were found by small signal analysis are not correctly estimated. Even the centers of two large clusters do not show true zeros values. In the next step, we will examine the single-input multiple-output analysis for Kundur system.

The followings are the subject of future works.

- Employing other types of injection signals like SMSW and comparing the results with LLPRN signal.
- Designing new injection signals for zero estimation in case that the available injection signals (for poles) do not work well for zero estimation.
- We have many real data from WECC system which are obtained by brake tests, probing tests, etc. After getting results from simulated power system responses, we will work on the real data.

To make the study more comprehensive, the application of other identification techniques like ARMAX method will be investigated and a general comparison between the methods will be provided.

6. Conclusions

Increased penetration of intermittent renewables and integration of new controls functionalities are motivating the analysis of the power grid's fast dynamics from an input-output perspective. The focus of this project was, firstly, to characterize the input-output properties (specifically, zeros) of the power system's swing dynamics. Analytical characterizations of the zeros in terms of structural properties of the network were undertaken using the classical model, and additionally numerical computations were developed for more detailed models of test systems. Applications of the zeros-analysis were pursued in a preliminary way, in two directions: 1) model reduction to preserve input-output properties; and 2) estimation of zeros from synchrophasor data. As a whole, the project confirmed the importance of input-output properties in the analysis and control of fast power-grid dynamics, and elucidated the role of the structure and operating characteristics of the grid in deciding input-output properties (and their analysis/ estimation). While the project work established the importance of input-output analyses and introduced tools for achieving these analyses, these efforts are just a starting point toward a comprehensive formal and numerical analysis of input-output properties for realistic-scale power system models. In addition, the initial project was limited in scope in that it focused primarily on characterization of input-output properties, rather than design to achieving desirable properties. Important next steps toward designing input-output characteristics of the fast dynamics include: 1) developing general zero-preserving model-reduction algorithms, 2) addressing estimation of zeros from synchrophasor measurements in a systematic way, 3) developing quantitative bounds on and 4) pursuing control design to shape input-output properties of specified channels.

References

[1] Korba, Petr, Ernst Scholtz, Albert Leirbukt, and Kjetil Uhlen. "Combining forces to provide stability." *ABB Review* 3 (2007): 34-38.

[2] Ulbig, Andreas, Theodor S. Borsche, and Göran Andersson. "Analyzing Rotational Inertia, Grid Topology and their Role for Power System Stability." *IFAC-PapersOnLine* 48, no. 30 (2015): 541-547.

[3] Bose, Anjan. "Smart transmission grid applications and their supporting infrastructure." *IEEE Transactions on Smart Grid* 1, no. 1 (2010): 11-19.

[4] Chakrabortty, Aranya, and Pramod P. Khargonekar. "Introduction to wide-area control of power systems." In *American Control Conference (ACC), 2013*, pp. 6758-6770. IEEE, 2013.

[5] Anderson, Paul M., and Aziz A. Fouad. *Power system control and stability*. John Wiley & Sons, 2008.

[6] Schrader, Cheryl B., and Michael K. Sain. "Research on system zeros: a survey." *International Journal of control* 50, no. 4 (1989): 1407-1433.

[7] Martins, Nelson, Herminio JCP Pinto, and Leonardo TG Lima. "Efficient methods for finding transfer function zeros of power systems." *IEEE Transactions on Power Systems* 7, no. 3 (1992): 1350-1361.

[8] Verghese, George, Bernard Lévy, and Thomas Kailath. "A generalized state-space for singular systems." *IEEE Transactions on Automatic Control* 26, no. 4 (1981): 811-831.

[9] Misra, Pradeep, Paul Van Dooren, and Andras Varga. "Computation of structural invariants of generalized state-space systems." *Automatica* 30, no. 12 (1994): 1921-1936.

[10] Briegel, Benjamin, Daniel Zelazo, Mathias Bürger, and Frank Allgöwer. "On the zeros of consensus networks." In *Decision and Control and European Control Conference (CDC-ECC), 2011 50th IEEE Conference on*, pp. 1890-1895. IEEE, 2011.

[11] Herman, Ivo, Dan Martinec, and Michael Sebek. "Zeros of transfer functions in networked control with higher-order dynamics." *IFAC Proceedings Volumes* 47, no. 3 (2014): 9177-9182.

[12] Abad Torres, Jackeline, and Sandip Roy. "Graph-theoretic characterisations of zeros for the input–output dynamics of complex network processes." *International Journal of Control* 87, no. 5 (2014): 940-950.

[13] Abad Torres, Jackeline, and Sandip Roy. "Graph-theoretic analysis of network input–output processes: Zero structure and its implications on remote feedback control." *Automatica* 61 (2015): 73-79.

[14] Abad Torres, Jackeline, and Sandip Roy. "A two-layer transformation for characterizing the zeros of a network input-output dynamics." In *Decision and Control (CDC), 2015 IEEE 54th Annual Conference on*, pp. 902-907. IEEE, 2015.

[15] Sanchez-Gasca, Juan J., and Joe H. Chow. "Power system reduction to simplify the design of damping controllers for interarea oscillations." *IEEE Transactions on Power Systems* 11, no. 3 (1996): 1342-1349.

[16] Nabavi, Seyedbehzad, and Aranya Chakrabortty. "Topology identification for dynamic equivalent models of large power system networks." In *American Control Conference (ACC), 2013*, pp. 1138-1143. IEEE, 2013.

[17] Valdez, Justin, Xun Zhang, Jackeline Abad Torres, and Sandip Roy. "Fast fault location in power transmission networks using transient signatures from sparsely-placed synchrophasors." In *North American Power Symposium (NAPS), 2014*, pp. 1-6. IEEE, 2014.

[18] C. Osauskas, C. and A. Wood, ``Small-signal dynamic modeling of HVDC systems," *IEEE Trans. Power Del.*, vol. 18, no. 1, pp. 220–225, Jan. 2003.

[19] C. W. Taylor and S. Lefebvre, ``HVDC controls for system dynamic performance", *IEEE Trans on Power Systems*, vol. 6, no. 2, pp. 743-752, May 1991.

[20] K. Koorehdavoudi et al., ``Input-output characteristics of the power transmission network's swing dynamics." *55th IEEE Conference on Decision and Control (CDC)*, 2016.

[21] K. Koorehdavoudi et al., ``Input-Output Properties of the Swing Dynamics for Power Transmission Networks with HVDC Modulation." To appear in *Proceedings of the IFAC World Congress*, June 2017.

[22] Dorfler, Florian, and Francesco Bullo. "Synchronization and transient stability in power networks and nonuniform Kuramoto oscillators." *SIAM Journal on Control and Optimization* 50, no. 3 (2012): 1616-1642.

[23] Martins, Nelson, Herminio JCP Pinto, and Leonardo TG Lima. "Efficient methods for finding transfer function zeros of power systems." *IEEE Transactions on Power Systems* 7, no. 3 (1992): 1350-1361.

[24] Sannuti, Peddapullaiah, and Ali Saberi. "Special coordinate basis for multivariable linear systems—finite and infinite zero structure, squaring down and decoupling." *International Journal of Control* 45, no. 5 (1987): 1655-1704.

[25] Kundur, Prabha. *Power system stability and control*. Edited by Neal J. Balu, and Mark G. Lauby. Vol. 7. New York: McGraw-hill, 1994.

[26] P. Van Overschee and B. De Moor, Subspace Identification: Theory, Implementation, Application. Dordrecht, The Netherlands: Kluwer, 1996, pp. 95–134.

[27] N. Zhou, J. Pierre, and J. Hauer, "Initial results in power system identification from injected probing signals using a subspace method," IEEE Trans. Power Syst., vol. 21, no. 3, pp. 1296–1302, Aug. 2006.

[28] W. E. Larimore, "Canonical variate analysis in identification, filtering, and adaptive control," in Proc. 29th IEEE Conf. Decision Control, Dec. 1990, vol. 2, pp. 596–604

[29] M. Verhaegen, "Identification of the deterministic part of MIMO state space models given in innovations form from input-output data," Automatica, vol. 30, no. 1, pp. 61–74, Jan. 1994

[30] L. Ljung, System Identification: Theory for the User, 2nd ed. Englewood Cliffs, NJ: Prentice-Hall PTR, 1999

[31] N. Martins, P. C. Pellanda, and J. Rommes, "Computation of transfer function dominant zeros with applications to oscillation damping control of large power systems," IEEE Trans. Power Syst., vol. 22, no. 4, pp. 1218–1226, Nov 2007.

[32] L. Ljung, "Prediction error estimation methods", *Circuits Syst. Signal Process.*, vol. 21, no. 1, pp. 11-21, 2002.

[33] Ning Zhou et al. "Initial Results in Power System Identification From Injected Probing Signals Using a Subspace Method", IEEE TRANS ON POWER SYS, VOL. 21, NO. 3, AUG 2006